# Local measure of quantum effects in quantum dynamics

Vitaly Rassolov* and Sophya Garashchuk*

*Department of Chemistry and Biochemistry, University of South Carolina, Columbia, SC 29208, USA*

E-mail: rassolov@mailbox.sc.edu; garashchuk@sc.edu

**Abstract**

The Madelung-de Broglie-Bohm formulation of the Schrödinger equation casts the time-evolution of a wavefunction as dynamics of an ensemble of quantum, or Bohmian, trajectories, interacting via the non-local quantum potential. This trajectory perspective gives insight into the quantumness (or classicality) of a given system due to clear partitioning of the energy into classical and quantum components. Here, we propose a system-independent measure of the quantumness of dynamics, based on the energy time-change, referred to as 'quantum power'. This measure is local in the coordinate space. Based on applications to model chemical systems, we argue that during the transition from the quantum to classical regime, defined as compression of quantization, the quantum features in dynamics do not 'disappear' but are pushed forward in time. This feature may be used to gauge the validity of the semiclassical and other approximate dynamics approaches in applications to anharmonic systems.

# 1 Introduction

Recent developments in exact methods of quantum dynamics, e.g.,[1–8] enable description of large chemical systems with relatively mild approximations. The applicability of the approximate methods often depends on the degree of *quantumness* in the underlying dynamics. Many popular practical methods incorporate mild quantum effects at some level. One great example is the quasiclassical trajectory (QCT) dynamics, introduced in 1965 by Karplus et al.,[9] which incorporates *ad hoc* quantization of the energy and angular momentum of the initial state into the trajectory sampling. The remarkable success of the QCT method in reproducing the experimental data and quantum scattering calculations for the $H+H_2$ reaction,[10] inspired decades of development and applications of the QCT dynamics, which remains a standard tool of the reactive gas-phase dynamics, e.g.,[11–15] and, moreover, has spurred the development of quantum and semiclassical theories of chemical reactions and Gaussian wavepacket methods, e.g.[16–23] Enabled by the advances in quantum and mixed quantum-(semi)classical dynamics methods, e.g.,[24–26] and in the potential energy surface construction and on-the-fly electronic structure calculations, e.g.,[27–29] increasingly larger molecular systems fall into the scope of theoretical and computational studies. Thus, description of spatially localized parts of molecular systems at different theory levels (similar to ONIOM in the electronic structure theory[30]) according to the dynamics quantumness, becomes an important consideration in choosing an efficient dynamics method for good balance of accuracy and numerical cost.

It is, therefore, highly desirable to have a spatially localized theoretical 'measure' of the quantum effects on the dynamics. Since there are no unambiguous ways to separate an interacting quantum system into localized subsystems, such a measure would necessarily be non-unique. The freedom to choose a particular form for this measure can be used to make it practical, and to have a conveniently defined limiting values. Specifically, it is desirable for such a measure to vanish in the classical limit of large (compared to the energy quantization) energy, or large mass, or large (compared to the Plank's constant) action.

In this paper we present a candidate for the quantumness measure defined as the ratio of expectation values of two linear operators in Hilbert space; this object quantifies the change of local wavefunction energy with time, and is therefore referred as the *quantum power* denoted $\mathcal{Q}$. This definition makes $\mathcal{Q}$ formally independent of the representation, though it retains parametric dependence on the wavefunction phase. The quantum power is inspired by the quantum trajectory (**QT**) formalism[31,32] and is adapted to the QT 'descriptors', as well as to the usual Hilbert space representation. Besides the main goal of quantifying the local quantum effects in chemical systems, $\mathcal{Q}$ is useful in the analysis of approximations underlying the quantum dynamics approaches, including the semiclassical implementations of the QT dynamics developed in our groups.[33–35]

The QT formalism is reviewed in Section 2.1, and the quantumness measure is derived in Section 2.2. Applications to the popular one- and two-dimensional models and discussion of the revealed features in dynamics and challenges the approximate approaches may face, are presented in Section 3. Section 4 concludes.

# 2 Theory

## 2.1 Theoretical background

In this section we review the quantum trajectory formulation of the time-dependent Schrödinger equation (**TDSE**) and introduce objects relevant to the subsequent derivation of the quantum power measure. For simplicity, the formalism below is described in $N_d$ Cartesian coordinates, $\boldsymbol{x}$, with the diagonal form of the kinetic energy. Generalization of the QT formalism to the curvilinear coordinates has been described previously.[36,37] The gradient symbol denotes the vector of spatial derivatives, $\boldsymbol{\nabla} = [\partial/\partial x_1, \partial/\partial x_2, \dots]$. The arguments of functions are suppressed when unambiguous. The subscript $t$ indicates trajectory attributes: for example, $\boldsymbol{q}_t$ and $\boldsymbol{p}_t$ are, respectively, the position and momentum of a trajectory at time $t$. Large and small bold-face letters are used to denote matrices and vectors, respectively, including

matrices and vectors of functions. The transpose notation, changing a column vector into a row vector, is omitted as in $\boldsymbol{p} \cdot \boldsymbol{v} = \sum_i p_i v_i$. The 'hat' symbol indicates an operator, acting on all terms to the right, as in $\hat{\boldsymbol{\nabla}} SA = A\boldsymbol{\nabla} S + S\boldsymbol{\nabla} A$. The absence of a hat implies action on the first term after the derivative symbol only, as in $\boldsymbol{\nabla} \cdot \boldsymbol{p}\, S = S \sum_i \frac{\partial p_i}{\partial x_i}$. If the term(s) to the immediate right of the derivative symbol are enclosed in the parentheses, the derivative acts on all terms in the parentheses, as in $\boldsymbol{\nabla} \cdot (\boldsymbol{p} S) = \sum_i \frac{\partial (S p_i)}{\partial x_i}$.

### 2.1.1 The quantum trajectory formulation of the TDSE

The QT framework is based on the standard TDSE and the polar form of a wavefunction,[31,32]

$$\left( -\frac{\hbar^2}{2} \hat{\boldsymbol{\nabla}} \mathbf{M}^{-1} \hat{\boldsymbol{\nabla}} + V \right) \psi(\boldsymbol{x}, t) = \imath\hbar \frac{\partial}{\partial t} \psi(\boldsymbol{x}, t), \tag{1}$$

where $V \equiv V(\boldsymbol{x})$ is an external potential, referred to in the given context as *classical*. The particle masses are position-independent and form the diagonal matrix $\mathbf{M}$. For a wavefunction represented in the polar form,

$$\psi(\boldsymbol{x}, t) = |\psi(\boldsymbol{x}, t)| e^{\imath S(\boldsymbol{x}, t)/\hbar}, \quad S(\boldsymbol{x}, t) \in \mathbb{R}, \tag{2}$$

application of the momentum operator $\hat{\boldsymbol{p}}$ yields:

$$\hat{\boldsymbol{p}} \psi = (-\imath\hbar \boldsymbol{r} + \boldsymbol{p}) \psi. \tag{3}$$

The vectors $\boldsymbol{p} \equiv \boldsymbol{p}(\boldsymbol{x}, t)$ and $\boldsymbol{r} \equiv \boldsymbol{r}(\boldsymbol{x}, t)$ are interpreted as *classical* and *nonclassical* momentum components, respectively,

$$\boldsymbol{p} := \boldsymbol{\nabla} S(\boldsymbol{x}, t), \tag{4}$$

$$\boldsymbol{r} := \frac{\boldsymbol{\nabla} |\psi(\boldsymbol{x}, t)|}{|\psi(\boldsymbol{x}, t)|}, \tag{5}$$

and the velocity vector is straightforwardly related to the classical momentum,

$$\boldsymbol{v} := \mathbf{M}^{-1}\boldsymbol{p}. \tag{6}$$

Using Eqs (2–6) in the TDSE (1), one obtains the continuity equation for the probability density $\rho \equiv \rho(\boldsymbol{x}, t)$,

$$\rho := |\psi(\boldsymbol{x}, t)|^2, \tag{7}$$

and the quantum Hamilton-Jacobi equation for $S(\boldsymbol{x}, t)$. Relating the phase gradient to the momentum of a *quantum* trajectory at the position $\boldsymbol{q}_t$,

$$\boldsymbol{p}_t := \boldsymbol{\nabla} S(\boldsymbol{x}, t)|_{\boldsymbol{x}=\boldsymbol{q}_t}\,, \tag{8}$$

the Lagrangian frame-of-reference is specified by the velocity of a QT,

$$\frac{d\boldsymbol{q}_t}{dt} = \boldsymbol{v}_t, \quad \boldsymbol{v}_t = \mathbf{M}^{-1}\boldsymbol{p}_t. \tag{9}$$

To streamline the notation, henceforth, the point for which expressions are evaluated is labeled as a subscript, e.g.

$$\boldsymbol{\nabla} S_{\boldsymbol{q}_t} := \boldsymbol{\nabla} S(\boldsymbol{x}, t)|_{\boldsymbol{x}=\boldsymbol{q}_t}\,.$$

Along the QT the wavefunction phase $S_t$ and the trajectory momentum $\boldsymbol{p}_t$ evolve according to:

$$\frac{dS_t}{dt} = \frac{\boldsymbol{p}_t \cdot \boldsymbol{v}_t}{2} - (V+U)_{\boldsymbol{q}_t}, \tag{10}$$

$$\frac{d\boldsymbol{p}_t}{dt} = -\boldsymbol{\nabla}(V+U)_{\boldsymbol{q}_t}. \tag{11}$$

The only difference between the quantum Hamilton-Jacobi Eq. (10) and its classical counterpart (and between following from them equations of trajectory motion (9,11)) is the

time-dependent *quantum* potential, $U \equiv U(\boldsymbol{x}, t)$, which we find convenient to express in terms of the nonclassical momentum $\boldsymbol{r}$,

$$U := -\frac{\hbar^2}{2}\left(\boldsymbol{r}\mathbf{M}^{-1}\boldsymbol{r} + \boldsymbol{\nabla}(\mathbf{M}^{-1}\boldsymbol{r})\right). \tag{12}$$

$U$ generates the quantum behavior of a system by coupling the QTs, collectively representing a wavefunction as an ensemble, through the non-local quantum force, $F^q = -\boldsymbol{\nabla}U_{\boldsymbol{q}_t}$. In the classical limit of $\hbar \to 0$, or heavy particle limit, $U$ formally becomes small in the absence of singularities. Discussion of the classical limit subtleties is deferred to Section 3.4.

Note, that the continuity equation for the probability density, which in the Lagrangian framework reads,

$$\frac{d\rho_t}{dt} - (\boldsymbol{\nabla}\cdot\boldsymbol{v})_{\boldsymbol{q}_t}\rho_t = 0, \tag{13}$$

does not explicitly depend on $U$ and, in general, is not unique to the QT dynamics. Alternatively, Eq. (13) can be expressed in terms of an additional QT 'descriptor' $h_t$ ($\boldsymbol{r} = \boldsymbol{\nabla}h$),

$$h_t := \ln|\psi(\boldsymbol{q}_t)|, \quad \frac{dh_t}{dt} = -\frac{1}{2}(\boldsymbol{\nabla}\cdot\boldsymbol{v})_{\boldsymbol{q}_t}. \tag{14}$$

Eq. (14) is used in numerical work of Section 3. As follows from Eqs (9) and (13), $\rho_t$ within the volume element $\delta\boldsymbol{x}_t$, associated with a QT at a position $\boldsymbol{q}_t$, is conserved in time,[33]

$$w := \rho_t\delta\boldsymbol{x}_t = \rho_0\delta\boldsymbol{x}_0 \quad \text{or} \quad \frac{dw}{dt} = 0. \tag{15}$$

Thus, in principle knowledge of the trajectory positions – more precisely of the associated volume elements $\delta\boldsymbol{x}_t$ – is sufficient to determine $\rho_t$ at $\boldsymbol{q}_t$. Thanks to the property (15), upon discretization of $\psi(\boldsymbol{x}, 0)$ in terms of $N_{tr}$ trajectories, a set of time-independent QT *weights*,

$\{w^{(n)}\}$, provides an easy way of computing the expectation values as ensemble averages,

$$\langle\hat{\mathcal{O}}\rangle_t = \int \mathcal{O}(\boldsymbol{x},t)|\psi(\boldsymbol{x},t)|^2 d\boldsymbol{x} \approx \sum_{n=1}^{N_{tr}} w^{(n)}\mathcal{O}(\boldsymbol{q}_t^{(n)}). \tag{16}$$

Finally, the energy of a QT, $\{\boldsymbol{q}_t, \boldsymbol{p}_t\}$, is naturally defined as,

$$E(\boldsymbol{q}_t) = \frac{1}{2}\boldsymbol{p}_t\ \mathbf{M}^{-1}\boldsymbol{p}_t + V_{\boldsymbol{q}_t} + U_{\boldsymbol{q}_t}. \tag{17}$$

To summarize, given the trajectory momentum definition (8), the quantum Hamilton-Jacobi Eq. (9), formally equivalent to the TDSE, defines the QT dynamics. The quantum features of the dynamics enter this formulation through the non-local quantum potential, which couples motion of trajectories within the ensemble representing a wavefunction. Thanks to the probability density continuity, Eq. (13), the QT ensemble gives an ideally compact representation of a wavefunction, but exact numerical implementation of the QT dynamics (Eqs (9–12)), generally hindered by the singularities in $U$ and $\boldsymbol{\nabla}U$ at the wavefunction nodes, is highly challenging.[38–41] This shortcoming is conceptually related to the computational complexity of the TDSE for general coupled potentials.[42,43] Nevertheless, the QT framework is useful in developing the approximate and quantum/classical methods,[44,45] including those for nonadiabatic dynamics in configuration and extended spaces,[46–50] and in interpreting the wavefunctions and the quantum phenomena in general.[51–55]

### 2.1.2 Time-dependent Gaussian window function

The quantum power measure will be defined by employing a Gaussian window-function,

$$g(\boldsymbol{x};\boldsymbol{q}_t,\mathbf{B}_t) = \exp\left(-(\boldsymbol{x}-\boldsymbol{q}_t)\mathbf{B}_t(\boldsymbol{x}-\boldsymbol{q}_t)\right), \tag{18}$$

centered at a QT position, evolving as defined by Eqs (8) and (9). The time-dependent *width* parameters of $g$ form a symmetric positive definite matrix, $\mathbf{B}$, whose dynamics comes from

the equations of motion of the Thawed Gaussian, i.e. Eq. (65),

$$\frac{d}{dt}\mathbf{B}_t = -\left(\mathbf{B}_t[\boldsymbol{\nabla}\otimes\boldsymbol{v}] + [\boldsymbol{\nabla}\otimes\boldsymbol{v}]^T\mathbf{B}_t\right)_{\boldsymbol{q}_t}. \tag{19}$$

In Eq. (19) and henceforth $[\boldsymbol{f}_1\otimes\boldsymbol{f}_2]$ denotes a matrix resulting from the tensor product of two vectors, $\boldsymbol{f}_1$ and $\boldsymbol{f}_2$. The Thawed Gaussian, popularized in chemical dynamics by Heller and co-workers,[56,57] is an exact solution to the TDSE in a parabolic potential,[58] summarized for reference in Appendix 5. The Gaussian of Eq. (18) integrates to $N_g$,

$$N_g := \left(\frac{\pi^{N_d}}{\det\mathbf{B}_t}\right)^{1/2} \sim \delta\boldsymbol{x}_t, \tag{20}$$

proportional to the volume element $\delta\boldsymbol{x}_t$ associated with the QT, as seen from the following arguments. If the width matrix is diagonal ($\mathbf{B}^d$), then the evolution of $N_g$ gives (Eq. (65)),

$$\frac{d}{dt}\sqrt{\det\mathbf{B}^d} = \frac{1}{2}\sum_\nu \frac{db_{\nu\nu}/dt}{b_{\nu\nu}}\sqrt{\det\mathbf{B}^d} = \frac{1}{2}\sum_\nu\left(-2\frac{\partial v_\nu}{\partial x_\nu}\right)\sqrt{\det\mathbf{B}^d} = -\boldsymbol{\nabla}\cdot\boldsymbol{v}\sqrt{\det\mathbf{B}^d}. \tag{21}$$

Eq. (21) is of the same form as Eq. (13) describing the time-dependence of $\rho_t$. Given that any symmetric positive definite matrix can be transformed into the diagonal form via (time-dependent) unitary transformation described by a matrix $\mathbf{T}$, $\det\mathbf{T}\equiv 1$, the proof above holds for the non-diagonal $\mathbf{B}$: $\det\mathbf{B} = \det(\mathbf{T}^{-1})\det\mathbf{B}^d\det\mathbf{T} = \det\mathbf{B}^d$. Because the QT weight given by Eq. (15) is conserved in time, the width matrix determinant is related to the volume associated with the QT: $(\det\mathbf{B}_t)^{-1/2}\sim\delta\boldsymbol{x}_t$.

## 2.2 Operators for the local energy and the measure of quantum power

### 2.2.1 The quantum trajectory operator

Let us introduce a Hermitian operator whose expectation value and evolution define a QT in the coordinate space. This operator, $g_W$, is defined as the limiting form of the Gaussian window-function of Section 2.1.2,

$$g_W = \lim_{\epsilon \to 0} \exp\left( -\frac{1}{\epsilon} (\boldsymbol{x} - \boldsymbol{q}_t) \mathbf{B}_t (\boldsymbol{x} - \boldsymbol{q}_t) \right). \tag{22}$$

Its expectation value vanishes at the specified limit as

$$\langle g_W \rangle = \lim_{\epsilon \to 0} \rho(\boldsymbol{q}_t) \sqrt{\frac{(\pi\epsilon)^{N_d}}{\det \mathbf{B}_t}}, \tag{23}$$

which is consistent with the concept of an individual trajectory having an infinitesimally small weight $w$ (Eq. (15)) in the limit of exact representation of a wavefunction, because $w \sim \delta\boldsymbol{x}_0$. The limit $\epsilon \to 0$ is understood to be taken after the expectation value is computed.

For convenience of working with normalizable functions, we also define the normalizable form of the single *trajectory operator* $g_W^\epsilon$,

$$g_W^\epsilon := \left( \frac{1}{\epsilon} \right)^{N_d/2} g_W. \tag{24}$$

The operator $g_W^\epsilon$ is essentially the $\delta-$function, based on a narrow Gaussian normalized to $N_g$ of Eq. (20), which represents a QT located at $\boldsymbol{q}_t$, its weight rescaled by the reciprocal of the initial discretization volume $\delta\boldsymbol{x}_0 = \epsilon^{N_d/2}$. In this sense, the limit variable $\epsilon$ corresponds to the square root of the average initial discretization volume around a trajectory of interest. We will be working with the operator $g_W^\epsilon$ understanding that it needs to be rescaled by the time-independent factor $\epsilon^{N_d/2}$ to represent an actual QT.

Leaving the overall normalization issue aside, we now show that the expectation value of this operator is time-independent:

$$\frac{\partial}{\partial t}\langle g_W^\epsilon\rangle = \langle\frac{\partial\psi}{\partial t}g_W^\epsilon\psi\rangle + \langle\psi\frac{\partial g_W^\epsilon}{\partial t}\psi\rangle + \langle\psi g_W^\epsilon\frac{\partial\psi}{\partial t}\rangle = \frac{-\imath}{\hbar}\langle\psi[g_W^\epsilon,\hat{H}]\psi\rangle + \langle\psi\frac{\partial g_W^\epsilon}{\partial t}\psi\rangle. \tag{25}$$

The first term in the last rhs of Eq. (25) contains the commutator $[g_W^\epsilon,\hat{H}]$. Because $g_W^\epsilon$ is multiplicative in coordinate space, it commutes with the potential energy portion of $\hat{H}$. Before proceeding with the kinetic energy operator, let us introduce the following notations for the mass-scaled gradient and the Laplacian,

$$_m\hat{\boldsymbol{\nabla}} := \mathbf{M}^{-1}\hat{\boldsymbol{\nabla}}, \tag{26}$$

$$\hat{\Delta} := \hat{\boldsymbol{\nabla}}\mathbf{M}^{-1}\hat{\boldsymbol{\nabla}}. \tag{27}$$

The wavefunction in polar form is denoted as follows:

$$\psi = \mathcal{A}\exp(\imath S/\hbar), \quad \mathcal{A} := |\psi| \tag{28}$$

With that, the kinetic energy part of the commutator becomes,

$$\frac{-\imath}{\hbar}\langle\psi[g_W^\epsilon,\hat{H}]\psi\rangle = \frac{\imath\hbar}{2}\langle\psi\left[g_W^\epsilon,\hat{\Delta}\right]\psi\rangle = -N_g\left(\mathcal{A}^2\Delta S + 2\mathcal{A}(\boldsymbol{\nabla}\mathcal{A}\cdot_m\boldsymbol{\nabla}S)\right)_{\boldsymbol{q}_t} + O(\epsilon). \tag{29}$$

The last term in Eq. (25) is computed from the time-dependence of the parameters of $g_W^\epsilon$ (Eqs (9) and (19)):

$$\begin{aligned}\langle\psi|\frac{\partial g_W^\epsilon}{\partial t}|\psi\rangle &= \frac{1}{\epsilon}\langle\psi|\left(\boldsymbol{v}_t\mathbf{B}_t(\boldsymbol{x}-\boldsymbol{q}_t) + (\boldsymbol{x}-\boldsymbol{q}_t)\mathbf{B}_t\boldsymbol{v}_t\right)g_W^\epsilon|\psi\rangle - \frac{1}{\epsilon}\langle\psi|(\boldsymbol{x}-\boldsymbol{q}_t)\frac{d\mathbf{B}_t}{dt}(\boldsymbol{x}-\boldsymbol{q}_t)g_W^\epsilon|\psi\rangle \\ &= N_g\left(2\mathcal{A}(\boldsymbol{\nabla}\mathcal{A}\cdot_m\boldsymbol{\nabla}S) + \mathcal{A}^2\Delta S\right)_{\boldsymbol{q}_t} + O(\epsilon).\end{aligned} \tag{30}$$

Together, Eqs (29) and (30) cancel each other through $O(1)$ and have $O(\epsilon)$ dependence on

the operator width. At the limit $\epsilon \to 0$ the time dependence of its expectation value vanishes,

$$\frac{\partial}{\partial t}\langle g_W^\epsilon \rangle = 0. \tag{31}$$

### 2.2.2 The local energy operator

Since the QT operator $g_W^\epsilon$ is multiplicative in coordinate space, it is logical to define a local, or 'window', energy operator as the Hermitized product of $g_W$ with the Hamiltonian,

$$\hat{E}_W := \frac{-\hbar^2}{4}(g_W\hat{\Delta} + \hat{\Delta}g_W) + V(\boldsymbol{x})g_W. \tag{32}$$

Its expectation value vanishes at the proper $\epsilon \to 0$ limit, similar to the case of $g_W$. Thus, it is convenient to define the normalizable form for $\hat{E}_W$,

$$\hat{E}_W^\epsilon := \left(\frac{1}{\epsilon}\right)^{N_d/2} \hat{E}_W. \tag{33}$$

Let us investigate its properties by computing its expectation value first:

$$\langle \hat{E}_W^\epsilon \rangle = N_g \left( \mathcal{A}^2 V + \frac{\mathcal{A}^2}{2}(\boldsymbol{\nabla} S \cdot_m \boldsymbol{\nabla} S) - \frac{1}{2}\mathcal{A}\Delta\mathcal{A} \right)_{\boldsymbol{q}_t} + O(\epsilon). \tag{34}$$

Interpreting this result as the total energy of a QT within the window function, the QT energy is computed by dividing $E_W^\epsilon$ by the trajectory weight and taking the limit $\epsilon \to 0$,

$$E(\boldsymbol{q}_t) = \frac{\langle \hat{E}_W^\epsilon \rangle}{\langle g_W^\epsilon \rangle} = \frac{\langle \hat{E}_W \rangle}{\langle g_W \rangle} = V(\boldsymbol{q}_t) + \frac{\boldsymbol{p}_t \cdot \boldsymbol{v}_t}{2} + U(\boldsymbol{q}_t), \tag{35}$$

in agreement with the Bohmian energy of Eq. (17). Note that the result is independent of the overall normalization of the QT operator $g_W$.

Next, let us turn to the time dependence of the local energy $\langle \hat{E}_W^\epsilon \rangle$,

$$\frac{\partial}{\partial t}\langle \hat{E}_W^\epsilon \rangle = \langle \frac{\partial \psi}{\partial t}\hat{E}_W^\epsilon \psi \rangle + \langle \psi \frac{\partial \hat{E}_W^\epsilon}{\partial t}\psi \rangle + \langle \psi \hat{E}_W^\epsilon \frac{\partial \psi}{\partial t} \rangle = \frac{-\imath}{\hbar}\langle \psi [\hat{E}_W^\epsilon, \hat{H}]\psi \rangle + \langle \psi \frac{\partial \hat{E}_W^\epsilon}{\partial t}\psi \rangle. \tag{36}$$

The terms in the expression above can be partitioned according to their dependence on the external potential $V$, since both the Hamiltonian and the local energy operators contain the terms proportional to $V$ and the terms independent of it. According to the derivation similar to that of Section 2.2.1 and detailed in Appendix 5, the time-derivative of $E_W^\epsilon$ simplifies to a *system-independent* expression – in other words, it does not explicitly depend on the external potential $V$:

$$\frac{\partial}{\partial t}\langle \hat{E}_W^\epsilon \rangle = \hbar^2 N_g \Big( 2\mathcal{A}(\Delta(\boldsymbol{\nabla} S \cdot_m \boldsymbol{\nabla}\mathcal{A})) - \Delta\mathcal{A}(\boldsymbol{\nabla} S \cdot_m \boldsymbol{\nabla}\mathcal{A}) \tag{37}$$
$$- \quad 2\mathcal{A}\ \mathrm{Tr}(\mathbf{M}^{-1}[\boldsymbol{\nabla}\otimes\boldsymbol{\nabla}\mathcal{A}]\mathbf{M}^{-1}[\boldsymbol{\nabla}\otimes\boldsymbol{\nabla}S]) + \frac{\mathcal{A}^2}{2}\Delta\Delta S - \mathcal{A}(\boldsymbol{\nabla} S \cdot_m \boldsymbol{\nabla})\Delta\mathcal{A}\Big)_{\boldsymbol{q}_t}$$

### 2.2.3 Definition of the Quantum Power

Using Eq. (37) along with Eqs (4, 12, 31), the time-derivative of the QT energy given by Eq. (35), or the *quantum power*, $\mathcal{Q}$, along the QT, defined as,

$$\mathcal{Q} := \frac{\partial}{\partial t}\left(\frac{\langle \hat{E}_W \rangle}{\langle g_W \rangle}\right) = \frac{\partial_t \langle \hat{E}_W^\epsilon \rangle}{\langle g_W^\epsilon \rangle}, \tag{38}$$

is equal to:

$$\mathcal{Q} = \Big( -(\boldsymbol{p}\cdot_m \boldsymbol{\nabla} U) + \hbar^2\,\mathrm{Tr}(\mathbf{M}^{-1}[(\boldsymbol{r}+\boldsymbol{\nabla})\otimes\boldsymbol{r}]\mathbf{M}^{-1}[\boldsymbol{\nabla}\otimes\boldsymbol{p}]) + \hbar^2(\boldsymbol{r}\cdot_m\boldsymbol{\nabla})\Delta S + \frac{\hbar^2}{4}\Delta\Delta S\Big)_{\boldsymbol{q}_t}. \tag{39}$$

For $\psi$ written in standard form, Eq. (39) is equivalent to

$$\mathcal{Q} = \frac{\hbar^2}{4|\psi|^2_{\boldsymbol{q}_t}}\Big( \Im\left(\psi^*\Delta\Delta\psi\right) - 2\Re\Big(\boldsymbol{p}\cdot_m\boldsymbol{\nabla}(\psi^*\Delta\psi) + \psi^*\Delta S\Delta\psi\Big)\Big)_{\boldsymbol{q}_t}. \tag{40}$$

The quantum power expressions (39) and (40), based on the system-independent definition of the local energy of Eq. (35), are the main analytic results of this Section. We note that, like the quantum potential $U$ of Eq. (12), $\mathcal{Q}$ is formally proportional to $\hbar^2$ and, therefore, vanishes in the classical limit (in the absence of singularities). For a Gaussian

wavepacket, the phase $S$ is quadratic in $\boldsymbol{x}$, which restricts $Q$ to a quadratic function of coordinates.

The quantum power expression Eq. (38) is based on the time dependence of the expectation values of the Hermitian operators $\hat{E}_W^\epsilon$ and $g_W^\epsilon$. While these operators depend on the phase of the wavefunctions through the window-function parameters $\mathbf{q}_t$ and $\mathbf{B}_t$ (Eq. (22)), they are defined in Hilbert space. Thus, $\hat{E}_W^\epsilon$ and $g_W^\epsilon$ can be evaluated in any representation, such as coordinate, momentum, expansion in the basis, etc. Moreover, the "quantumness" measure $\mathcal{Q}$ is established without *a priori* separation of energy into the "classical" and "quantum" parts. Therefore, we expect $\mathcal{Q}$ to be applicable and useful in the context of any quantum dynamics methods, not just those involving the quantum potential defined by Eq. (12). Other useful local quantities can be derived similar to $\mathcal{Q}$ by computing the expectation value of the symmetrized product of the corresponding operator with $g_W$, as done in Eq. (32). The properties of $g_W$, in particular, the time-independence of $\langle g_W^\epsilon \rangle$ (Eq. (31)) demonstrated in Section 2.2.1 is crucial for this. This paper, however, is limited to the analysis of $\mathcal{Q}$. The results based on the informative model systems are presented in the next Section.

# 3 Results and discussion

Before proceeding with the applications, let us note, that evaluation of $\mathcal{Q}$ and construction of the QTs are numerically challenging in systems whose dynamics is dominated by interference effects, because the singularities in the wavefunction amplitude and phase, associated with the wavefunction nodes, are amplified in the computations of the second-fourth order spatial derivatives of $|\psi|$ and $S$. We use Maple software for all models involving Gaussian wavepackets and plane waves, where $\mathcal{Q}$ can be evaluated and analyzed analytically, provided accurate numerical solutions of the equations of motion for the Gaussian wavepacket parameters. Selected Maple worksheets are available as Supplementary Information. For the Eckart barrier model, $\mathcal{Q}$ and the QTs are constructed from the time-dependent wavefunc-

tion computed on a dense spatial grid, employing the simplectic split-operator/Fast Fourier Transform (SOFT) propagator[59,60] with a time-step about ten times smaller compared to that of conventional wavefunction evolution. The atomic units ($\hbar = 1$) are used henceforth.

## 3.1 Harmonic oscillator

To facilitate the analysis of the quantum power $\mathcal{Q}$ let us start with the one-dimensional harmonic oscillator system, taking advantage of the analytic solution for the time-dependent Gaussian wavepacket (**GWP**) described in Appendix 5. The GWP exhibits two independent modes of motion: the translation of its center $\overline{\boldsymbol{x}}$ and, superimposed on it, the 'breathing' mode, determined by the time-dependence of the complex width parameter $\boldsymbol{A} = \boldsymbol{A}_{\Re} + \imath \boldsymbol{A}_{\Im}$. Adapted to one dimension, given the classical force constant $V_2 = m\omega^2$, the time-dependent GWP is

$$\psi(x,t) = N_0 \exp\left(-A(x-\overline{x}_t)^2/2 + \imath \overline{p}_t (x-\overline{x}_t) + \imath s_t + \gamma_t\right). \tag{41}$$

The prefactor $N_0 = (\Re(A_0)/\pi)^{1/4}$ normalizes the wavefunction to 1 at $t = 0$, and the initial values of the parameters $\gamma_0$, and $s_0$ are set to zero without loss of generality. For a particle of mass $m$ the quantum power becomes

$$\mathcal{Q} = \underbrace{\frac{A_{\Re}^2\, \overline{p}_t}{m^2}(x-\overline{x}_t)}_{\text{translation}} - \underbrace{\frac{A_{\Re} A_{\Im}}{m^2}\left(2A_{\Re}(x-\overline{x}_t)^2 - 1\right)}_{\text{breathing mode}}. \tag{42}$$

For a special choice of the initial GWP, i.e. $A_0 = m\omega/2$, the width parameter remains constant in time; such GWP is called coherent, and the wavepacket shape $|\psi(x,t)|$ remains 'frozen' in time. Using for simplicity $m = 1$, $\omega = 1$ and centering the potential at $x = 0$ (all in atomic units), the dynamics of the coherent GWP is limited to the translational motion and accumulation of the linear in $x$ phase; $\mathcal{Q}$ is simply a linear function of $x$ described by the first term of Eq. (42). The dynamics is illustrated in Fig. 1 for the GWP initialized as $A = 1$ $\mathrm{a}_0^{-2}$, $\overline{x}_0 = -2$ $\mathrm{a}_0$ and $\overline{p}_0 = 0$. Several snapshots of $\mathcal{Q}$ are superimposed on the QTs 'flowing'

in time (upwards on the plot): the line segments cross the corresponding GWP centers, and the slope of $\mathcal{Q}$ changes over the oscillator period $T_1 = 2\pi$ as $\overline{p}_t = -\overline{x}_0 \sin(t)$. For $t \in (0, \pi)$ the GWP gains energy to the right of its center (and looses to the left of the center) which corresponds to the GWP motion to the right; for $t \in (\pi, 2\pi)$ the energy change is reversed and the GWP moves to the left; $\mathcal{Q}$ is exactly zero when the wavepacket changes direction of its motion at $t = \{0, \pi, 2\pi\}$.

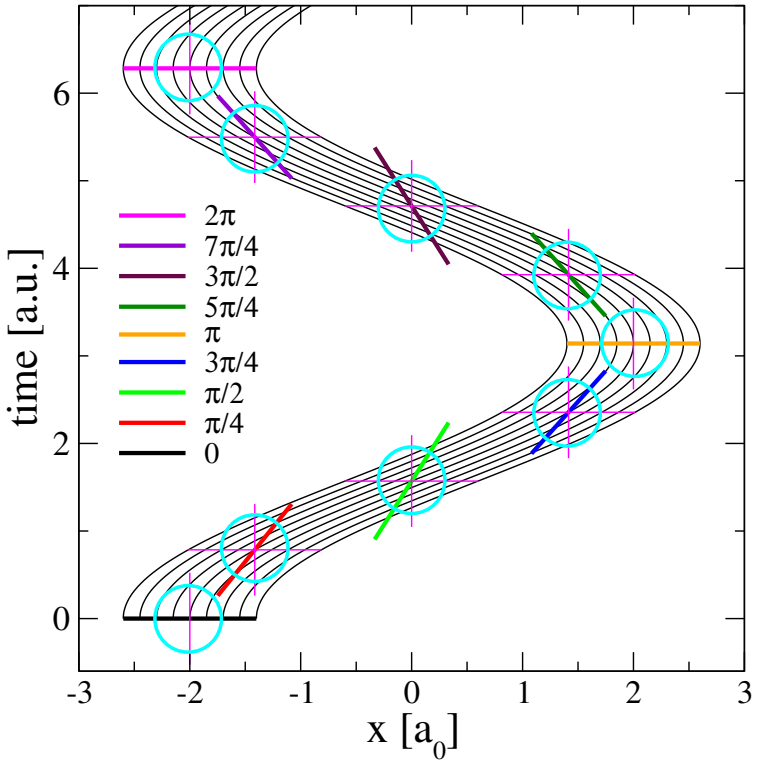


Figure 1: The translational motion of a coherent GWP in a parabolic potential. Time is measured along the vertical axis. The QTs, shown as thin solid lines, track the dynamics of the wavefunction, whose footprints are marked as circles. The corresponding $\mathcal{Q}$, is plotted as straight line segments for nine instances of time listed in the legend. For each $t$, thin magenta lines show the axes for $\mathcal{Q}$ (vertical) vs $(x - \overline{x}_t)$ (horizontal), where $\overline{x}_t$ denotes the GWP center.

To isolate the breathing mode, we start with the squeezed, compared to the coherent case, GWP at the bottom of the potential well: $A = 2\ \mathrm{a}_0^{-2}$, $\overline{x}_0 = 0$ and $\overline{p}_0 = 0$. In this case, $\mathcal{Q}$ is a parabola with the time-dependent curvature given by the second rhs term in Eq. (42). The time-dependence of $A$, which in this case fully defines the dynamics of $\mathcal{Q}$, is periodic on

$T_2 = \pi$. The snapshots of the GWP and $\mathcal{Q}$ are presented in Fig. 2, and the underlying QT dynamics is shown in Fig. 3(a). For the initially squeezed GWP, the energy flows from the center (the region of negative $\mathcal{Q}$) to the fringes of the wavepacket (the regions of positive $\mathcal{Q}$) until the maximum wavepacket delocalization is reached at $t = \pi/2$ a.u. At this time $\mathcal{Q} = 0$ and the QTs are maximally spread out. Then, the energy flow reverses its direction and proceeds from the fringes to the center until the initial width is reached at $t = \pi$.

For a general GWP, $\mathcal{Q}$ is a combination of both modes of motion resulting in a more complicated time-dependence of $\mathcal{Q}$; note that $\mathcal{Q}$ has different periods $T_1$ and $T_2$ for the transnational and breathing modes.

## 3.2 Interference

One of the well-known demonstrations of the quantum nature of particles is the double-slit experiment (e.g.[61]) revealing the interference patterns in the probability distribution. The QT dynamics describing quantum interference of Gaussian wavepackets has been described previously.[62,63] In this section, we focus on the rate of the energy change associated with interference.

### 3.2.1 Two GWPs

The complexity of $\mathcal{Q}$ grows significantly when wavefunction dynamics is characterized by interference. The QTs and $\mathcal{Q}$ describing interference of two coherent GWPs, are shown in Figs 3(b) and 4, respectively. The initial wavefunction is a *sum* of two displaced coherent GWPs, each described by Eq. (41) for the initial parameter values $A_0 = 1\ \mathrm{a}_0^{-2}$, $\overline{x} = \pm 2\ \mathrm{a}_0$ and $\overline{p} = 0$. In this model we observe the following dynamics features. (i) For $t = [0, \pi/2]$ the two GWPs accelerate towards each other and $|\psi(x,t)|$ develops the typical interference pattern shown in the upper row in Fig. 4. (ii) At $t = \pi/2$ the wavefunction exhibits maximum interference characterized by singularities in $r$ (middle row): $\psi \sim \exp(-x^2/2)\cos(2x)$, $r = -x - 2\tan(2x)$. Nevertheless, at this time $\mathcal{Q}$ is zero for all $x$ (bottom row) as the two GWPs

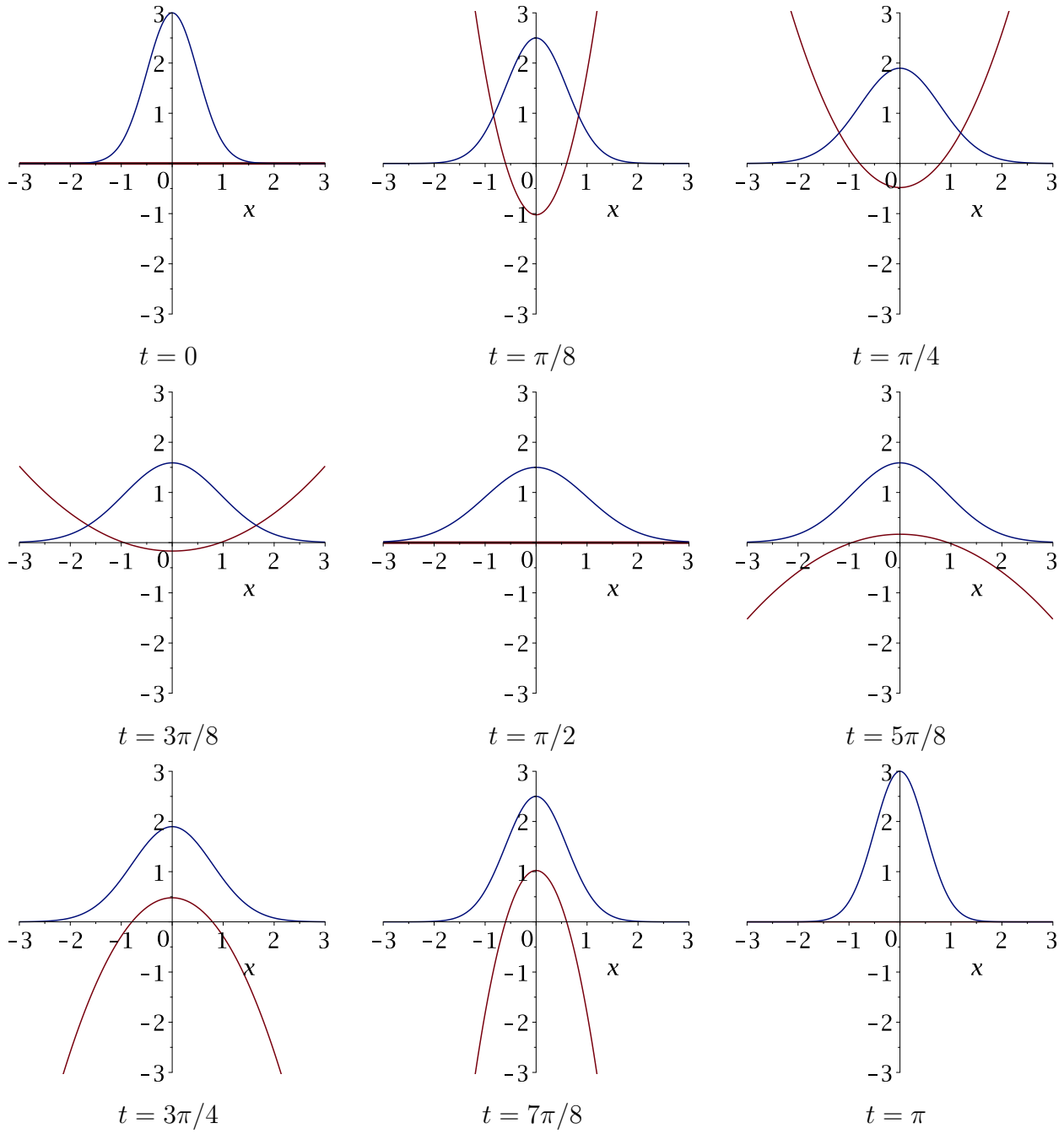


Figure 2: The GWP breathing mode. The snapshots of $\mathcal{Q}$ and $|\psi|$ are plotted for times indicated at the bottom of each panel. The vertical axis corresponds to $\mathcal{Q}$ in a.u. (parabolas shown as red lines); on the same vertical scale, the wavefunction modulus (Gaussian functions in blue) is multiplied by 2.68. The wavefunction is initialized as $\overline{x}_0 = 0$ a$_0$, $\overline{p}_0 = 0$ and $A_0 = 2$ a$_0^{-2}$.

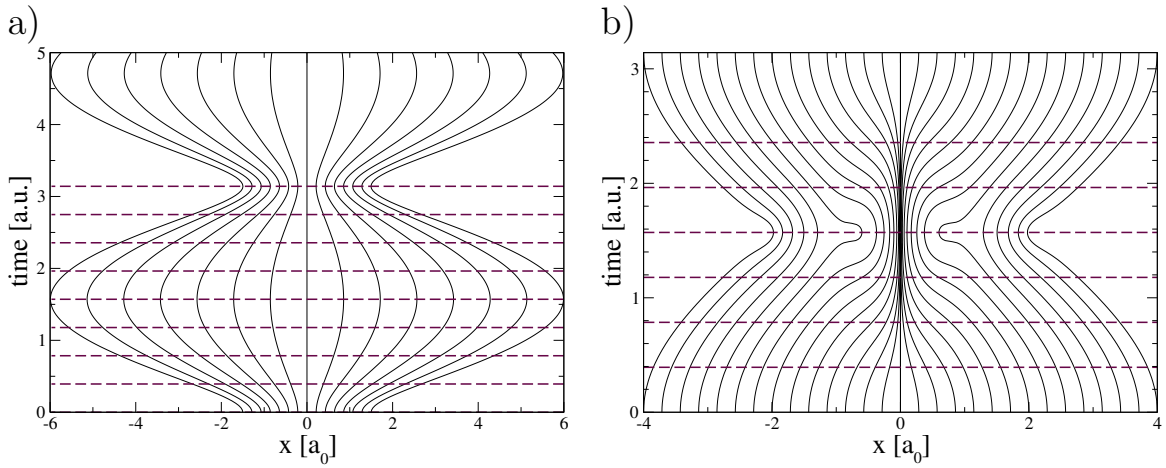


Figure 3: Evolution of the QT ensemble underlying (a) the breathing mode of the GWP dynamics in Fig. 2 and (b) the wavepacket interference dynamics in Fig. 4. Dashes indicate the time of snapshots presented in Figs 2 and 4. In panel (a) notice the instance of maximum wavepacket localization at $t = \pi$ for an initially squeezed GWP. In panel (b) the maximum wavepacket localization is achieved at $t = \pi/2$; the QTs go around the wavefunction nodes fully evolved at $x = \pm\pi/4$ a$_0$.

switch places. The smallest localization of $|\psi|$ at $t = \pi/2$ is seen in the minimal spread of QTs shown in Fig. 3(b); the maximum interference is manifested in the QTs circumventing the nodal region of $\psi$ at $x = \pm\pi/4$ a$_0$. (iii) Over the time interval $[\pi/2, \pi]$ the two GWPs separate, which is accompanied by $\mathcal{Q}$ changing its sign (compare $t = 5\pi/8$ and $t = 3\pi/8$ snapshots) and by the reversal of the dynamics compared to the $[0, \pi/2]$ time interval. At the wavefunction fringes the slope of $\mathcal{Q}$ corresponds to the direction of the GWP motion as in the case displayed in Fig. 1, while the oscillatory behavior in the middle is dominated by the dynamics of the peaks of $|\psi|$ including their positions and widths.

### 3.2.2 Two plane waves

The challenge of using the QT dynamics as a numerical tool comes from the fact that the quantum force does not vanish in the regions of low probability density, and is large near the wavefunctions nodes. Even if the quantum force is formally zero, as for example the case of excited eigenstates, this zero is achieved by cancellation of singularities of opposing signs. Therefore, to gain further insight into the role of the quantum energy in interference,

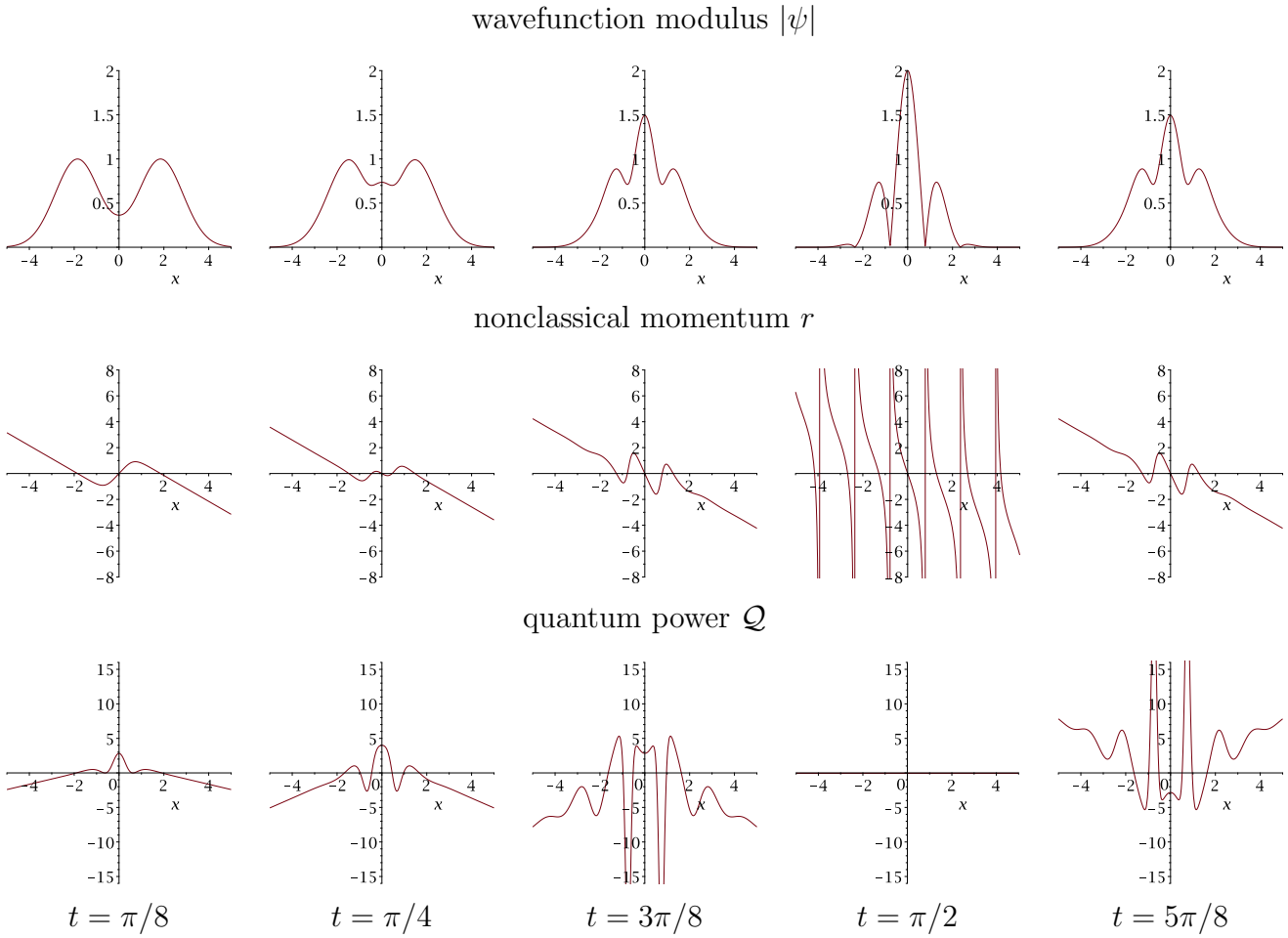


Figure 4: Interference of two coherent Gaussians, initialized as $\overline{x}_0 = \pm 2$ a$_0$, $\overline{p}_0 = 0$ and $A_0 = 1$ a$_0^{-2}$. The top, middle and bottom rows show $|\psi|$, $r$ and $\mathcal{Q}$, respectively, plotted at times, labeled at the bottom of each column, as a function of $x$, all in atomic units.

we proceed with the idealized model of this effect.

Let us consider a wavefunction composed of two plane waves with different momenta and amplitudes describing a particle of mass $m = 1$ a.u.,

$$\psi(\boldsymbol{x}, t) = C_1 \exp\left(\imath(\boldsymbol{p}_1\boldsymbol{x} - E_1 t)\right) + C_2 \exp\left(\imath(\boldsymbol{p}_2\boldsymbol{x} - E_2 t)\right) \tag{43}$$

Denoting the phase shift as $\Omega$,

$$\Omega := (E_1 - E_2)t - (\boldsymbol{p}_1 - \boldsymbol{p}_2)\boldsymbol{x}, \tag{44}$$

the probability density and the nonclassical and classical momenta are given by

$$\begin{aligned} \rho &= C_1^2 + C_2^2 + 2C_1C_2\cos\Omega \\ \boldsymbol{r} &= \rho^{-1}C_1C_2(\boldsymbol{p}_1 - \boldsymbol{p}_2)\sin\Omega \\ \boldsymbol{p} &= \rho^{-1}\left(C_1^2\boldsymbol{p}_1 + C_2^2\boldsymbol{p}_2 + C_1C_2(\boldsymbol{p}_1 + \boldsymbol{p}_2)\cos\Omega\right) . \end{aligned} \tag{45}$$

Substituting Eqs (45) into Eq. (39), the quantum power in this model is equal to:

$$\mathcal{Q} = \left(C_1C_2(C_1^2 - C_2^2)^2(\boldsymbol{p}_2^2 - \boldsymbol{p}_1^2)(\boldsymbol{p}_1 - \boldsymbol{p}_2)^2\sin\Omega\right)/(4\rho^3) . \tag{46}$$

This expression is periodic with the temporal frequency $E_1 - E_2$ and spatial frequency $\boldsymbol{p}_1 - \boldsymbol{p}_2$, consistent with the usual plane wave interference pattern. The expression is singular at the nodes formed when $C_1 = C_2$. To understand this singularity, let us define $C_2 = (1 + z)C_1$ and analyze its behavior as $z \to 0$. For small $z$, $\mathcal{Q}$ reaches its extrema at $\Omega_x = \pi \pm z/\sqrt{5}$,

$$\mathcal{Q}_x = \pm\frac{1}{z^3}(\boldsymbol{p}_1^2 - \boldsymbol{p}_2^2)(\boldsymbol{p}_1 - \boldsymbol{p}_2)^2\frac{25\sqrt{5}}{216} . \tag{47}$$

The points in coordinate space and time where the energy change is maximized are adjacent to the minima of the density $\rho^{\min} = C_1^2z^2$ at $\Omega = \pi$. The sharp $O(z^{-3})$ singularity presents

significant numerical challenge to the QT description of systems with spatial nodes. The superposition of two plane waves analyzed above is illustrated in Fig. 5 in one dimension, for the parameter values of $p_1 = -1$, $p_2 = 2$ a.u. and $C_1 = 1$, $C_2 = 1.4$. The $C_2$ value, chosen for visual clarity, is beyond the small $z$ approximation, and the presented functions $|\psi|^2$ and $\mathcal{Q}$ are computed exactly. As seen in Fig. 5(a), the QTs, initiated on an equidistant grid, flow around the low-density near-nodal features of the wavefunction located at $t = 0$ at $x = \pm\pi/3$ (Fig. 5(b)). This behavior corresponds to the prominent peaks in $\mathcal{Q}$ (Fig. 5(c)) even in this case of $z = 0.4$. These features drift to the right with constant velocity $v = 1/2$ a.u., as illustrated by the same functions, shown at $t = 1$ a.u. Note that individual QTs move differently. In this system they all move to the right with velocities ranging from 0.75 a.u. to 9.5 a.u. They experience the sharpest accelerations near the partial nodes of the wavefunction (Fig. 5(b)) by redistributing the quantum energy as shown in Fig. 5(c).

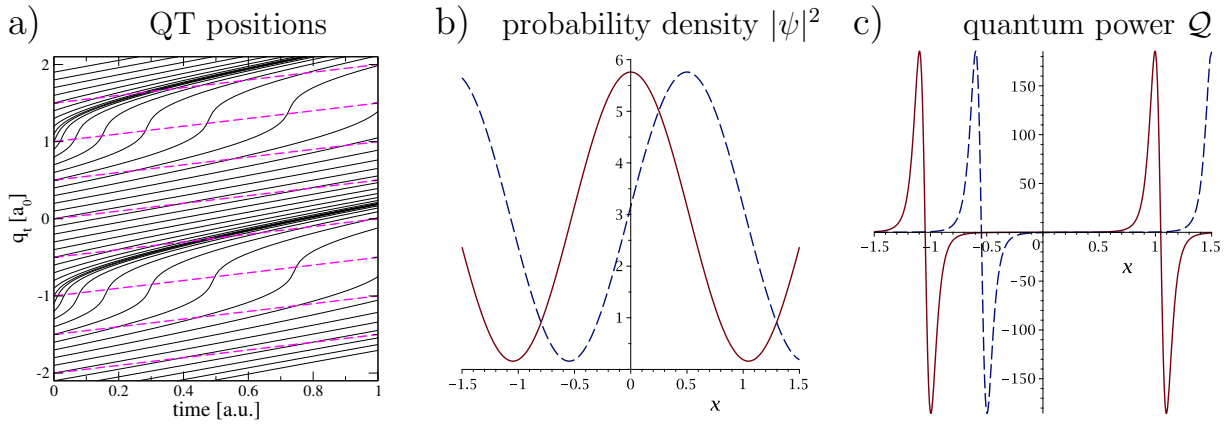


Figure 5: Plane wave interference in one dimension. The wavefunction parameters are given in the text. (a) The positions of the quantum trajectories, $\{q_t\}$ (vertical axis) are shown as functions of time (horizontal axis); magenta dashes show the drift of observable features such as those shown on the other panels. (b) The probability density, $|\psi|^2$, and (c) the quantum power, $\mathcal{Q}$, are shown as functions of coordinate $x$ at $t = 0$ and $t = 1$ (all in atomic units) as red solid lines and blue dashes, respectively.

## 3.3 Tunneling dynamics

In this section we examine dynamics dominated by tunneling, which can be viewed as the signature of quantum interference. We start with a popular benchmark potential, i.e. the Eckart barrier, mimicking the transition state of H+$H_2$ reaction, and proceed to an analytic two-state model for a closer examination of the deep-tunneling regime.

### 3.3.1 Scattering on the Eckart barrier

Wavepacket scattering on the Eckart barrier in one dimension is a typical model of a reactive system. The functional form is $V = V_0/\cosh(\eta x)^2$, where $V_0 = 16$ a.u., $\eta = 1.3624$ $a_0^{-1}$. These particular parameter values correspond to the transition state of H+$H_2$ rescaled to have the particle mass of $m = 1$ a.u.[33] The QTs shown in Fig. 6, describe dynamics of the wavepacket, initially localized in the reactant region, $x < 0$, to the left of the barrier. The underlying wavefunction is computed on an equidistant grid of 4096 points spanning the range $x = [-40, 40]$ $a_0$ using SOFT propagator with the time-step of $6.25 \times 10^{-5}$ a.u. The parameters in Eq. (41) are set to $A_0 = 1/2$, $\overline{x}_0 = -4$ and $\overline{p}_0 = 4$ a.u. The wavepacket energy is close to half the barrier height, thus bifurcation – the trajectory ensemble splits into the reflected and transmitted parts – is a prominent feature of the dynamics. Another noticeable feature is the oscillatory behavior of the bifurcating trajectory pairs, associated with the wavefunction reflection inside the barrier. In the figure, the batches of trajectories shown with different colors spin off the oscillating separatrix in both directions. Their dynamics underlies the interference pattern seen on both sides of the barrier, including low-amplitude interference on the product side ($x > 0$), as seen in Fig. 7(a) displaying $|\psi|$ on the logarithmic scale. The corresponding quantum power $\mathcal{Q}$, shown in Fig. 7(b-d), reveals an intriguing picture of the tunneling process. (i) On the reactant side of the barrier (Fig. 7(b)), $\mathcal{Q}$ displays the expected interference pattern (compare to the interference of two GWPs in Fig. 4), especially prominent at shorter times due to combination of the incoming and reflected components of $\psi$. (ii) There is a wavepacket bifurcation point near $x = 0$ at all times, where

$\mathcal{Q}$ changes sign from negative to positive ($t = \{1.51, 1.38, 1.84\}$ a.u.) as the transmitting part of $\psi$ is pushed to the product side, and from positive to negative near $x = -0.4$ $a_0$ at $t = 2.3$ a.u. as the reflecting part is pushed towards the reactant side; at $t = 1.61$ and $t = 2.07$ a.u., the amplitude of $\mathcal{Q}$ is very large ($|\mathcal{Q}| > 1500$) at the points of inside-the-barrier reflection seen near the QTs turning points $x \approx -0.4$ and $x \approx -0.2$ $a_0$, for the two times, respectively. (iii) On the product side of the barrier, associated with the purely transmitted waves, $\mathcal{Q}$ changes sign, as seen in Fig. 7(c-d), at the points related to the oscillatory behavior of the separatrix shown in Fig. 6.

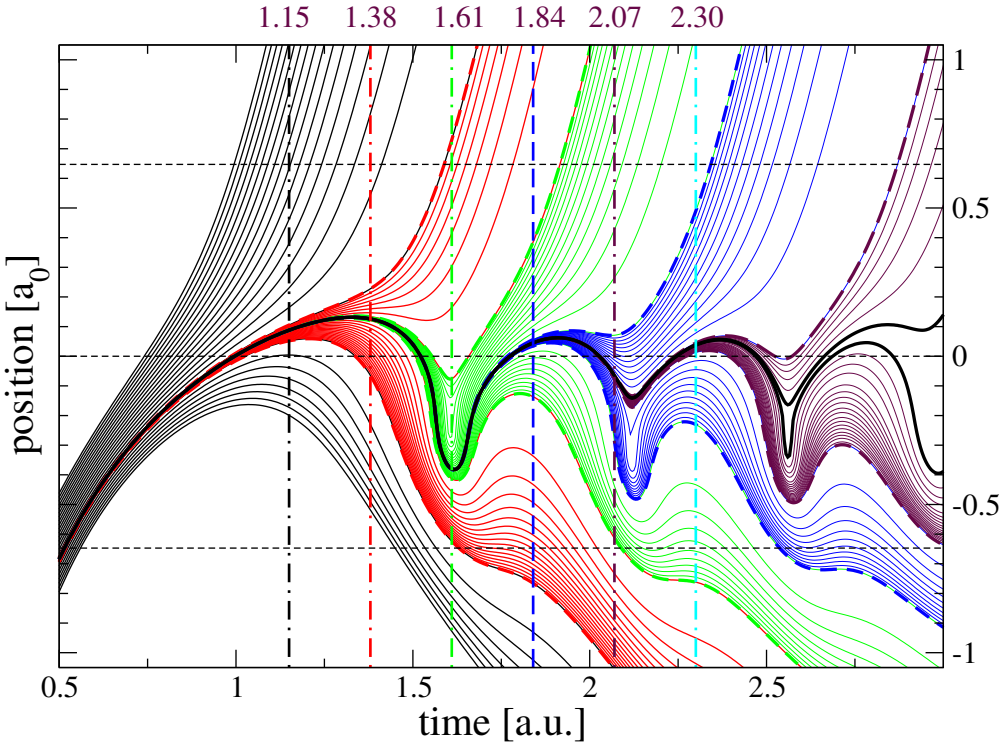


Figure 6: The wavepacket bifurcation on the Eckart barrier. The short dashes indicate the positions of the barrier half-height. Sets of trajectories of different colors (25 trajectories each) are initialized as insertions into the preceding bifurcating trajectory pair, highlighted with dashes. The order of colors is black, red, green, blue and maroon. The last bifurcating trajectory pair is marked with thick black lines. The vertical dot-dashes correspond to the times, indicated at the top of the graph, of snapshots of $|\psi|$ and $\mathcal{Q}$ displayed in Fig. 7.

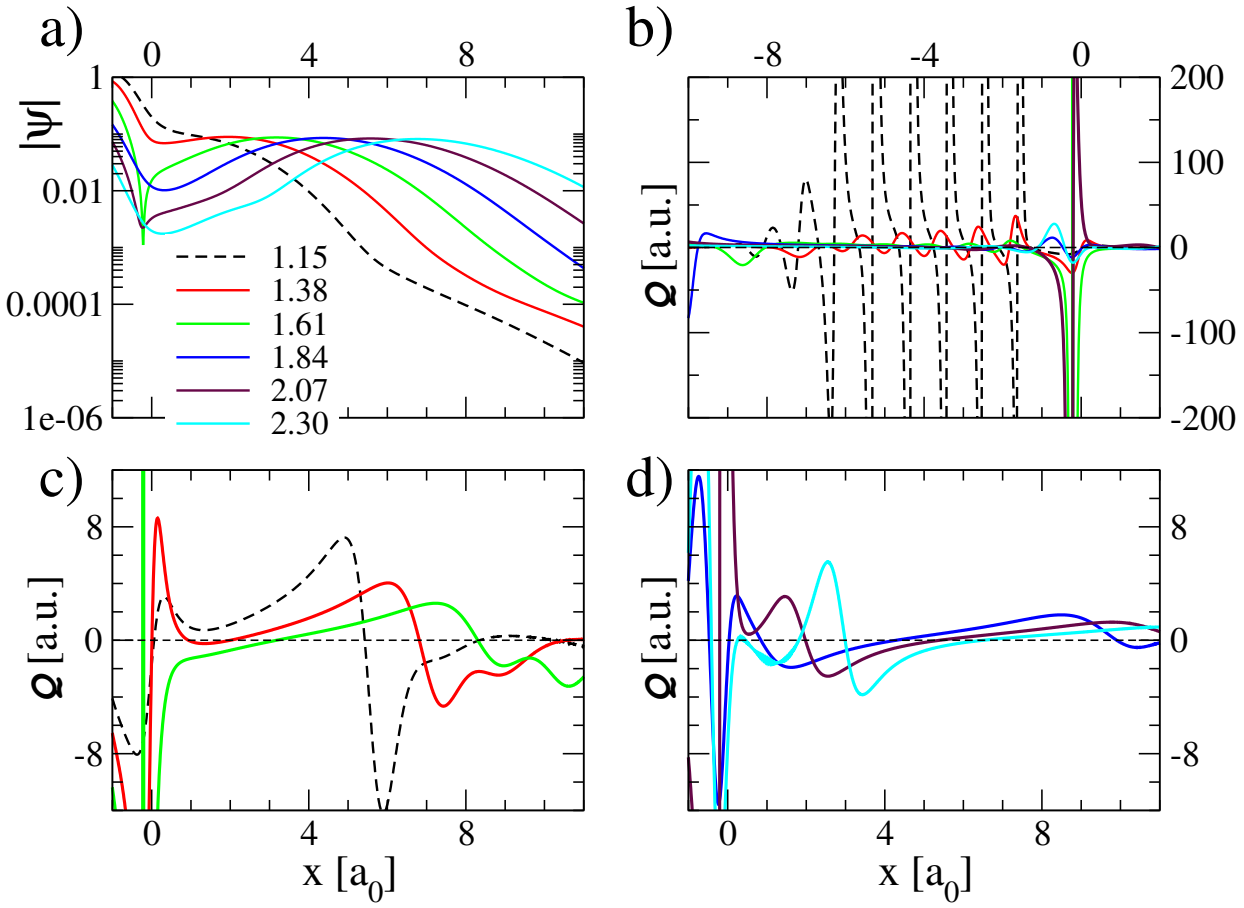


Figure 7: Scattering on the Eckart barrier. The snapshots of $|\psi(x,t)|$ (panel (a), logarithmic vertical scale) and $\mathcal{Q}$ (panels (b-d)) are shown for the times listed in a.u. on the legend applicable to all panels. The spatial regions of the energy gain/loss are the upper/lower half-plains separated by the short dash. Note the difference in vertical scale and shift in $x$-range in panel (b) corresponding to the reactant region, compared to panels (c-d) corresponding to the product region.

### 3.3.2 Analytic model: deep tunneling in the double well

To gain insight into the deep tunneling regime, let us consider the two-level system, as the limiting case of dynamics in a double-well potential representing a reaction in condensed phase. We define a time-dependent wavefunction in the configuration space as a superposition of two normalized Gaussians, $\chi_{R/L}$, of equal widths, $\alpha$, centered for simplicity at $\overline{x}_{R/L} = \pm 1$ a$_0$,

$$\chi_L = \left(\frac{\alpha}{\pi}\right)^{1/4} \exp\left(\frac{-\alpha(x+1)^2}{2}\right), \quad \chi_R = \left(\frac{\alpha}{\pi}\right)^{1/4} \exp\left(\frac{-\alpha(x-1)^2}{2}\right). \tag{48}$$

The diagonal elements of the Hamiltonian matrix are shifted to zero; its off-diagonal elements, dependent on the exact shape of the external double-well potential, are specified by the parameter $\varepsilon$, $\varepsilon = \langle \chi_L | \hat{H} | \chi_R \rangle$. The off-diagonal elements of the basis overlap matrix are denoted $\sigma$, $\sigma = \langle \chi_L | \chi_R \rangle = \exp(-\alpha)$. Introducing the dimensionless time $\tau$,

$$\tau := -\frac{2\sigma\varepsilon t}{1-\sigma^2}, \tag{49}$$

the solution to the TDSE, initially localized in the left basis function, takes the following form:

$$\psi(x,t) = \exp\left(\frac{\imath\varepsilon t}{1+\sigma}\right)\left(\frac{1+e^{\imath\tau}}{2}\chi_L + \frac{1-e^{\imath\tau}}{2}\chi_R\right). \tag{50}$$

The classical and nonclassical momentum components (Eqs (4) and (5)), defining $\mathcal{Q}$ of Eq. (39), are equal to:

$$\begin{aligned} p &= \frac{-2\alpha \sin\tau}{(1+\cos\tau)\zeta^{-1} + (1-\cos\tau)\zeta}, \quad \zeta := \exp(2\alpha x) \\ r &= -\alpha \frac{(1+\cos\tau)(x+1)\zeta^{-1} + (1-\cos\tau)(x-1)\zeta}{(1+\cos\tau)\zeta^{-1} + (1-\cos\tau)\zeta} \end{aligned} \tag{51}$$

We will focus on $\mathcal{Q}$ computed at two short values of the dimensionless time, $\tau = \pi/10000$ and $\tau = \pi/10$, for $\alpha = 5$ a$_0^{-2}$. Note that $\mathcal{Q} = 0$ at $\tau = n\pi$ ($n \in \mathbb{N}$), which defines $\pi$ as the

time-scale in this model. We also calculate $\mathcal{Q}$ without the third and fourth order derivatives in Eq. (39); the neglected terms would be equal to zero for a single GWP. This 'quadratic' approximation to $\mathcal{Q}$, is of interest, because the quantum potential based on the Gaussian approximation to $|\psi|$ has been explored by several research groups.[64–67]

A few time-snapshots of the wavefunction amplitude are shown in Fig. 8 on a logarithmic vertical scale. The wavefunction, initially a Gaussian centered at $\overline{x}_0 = -1$ $a_0$, is fully transferred to the right at $\tau = \pi$ and is equally distributed across the wells at $\tau = \pi/2$. In this deep-tunneling model, the wavefunction dynamics is markedly different compared to the Eckart barrier model: due to the bound character of the underlying double-well potential, the interference pattern moves from right (which is the low density region at $\tau = 0$) to left, as seen in the positions of node in $\mathcal{Q}$ shown in Fig. 8(b). The minimum of $|\psi|$ (Fig. 8(a)) is seen in the right well already at very short times, e.g. $|\psi| \sim 10^{-7}$ at $\tau = \pi/10^7$. Subsequently, the minimum shifts towards the barrier region of higher density.

Another observation is that the quadratic approximation to $\mathcal{Q}$ (associated with a Gaussian approximation to $\psi$) is poor in this system. It is qualitatively incorrect. At very short times the energy change exhibits large amplitude very far from the initial localization of $\psi$. As time moves forward, $\mathcal{Q}$ of high amplitude propagates from the distant wall of the right well towards the barrier. While most of the probability density and, thus, of QTs with non-zero weights, are located in the left well, the quantum energy redistribution occurs in the nearly empty right well. We interpret this as QTs being "pulled" through the potential barrier via the wavefunction tails. Practical description of such process via QT formalism requires pre-populating the empty well with QTs of negligible weights, which is consistent with very low tunneling probabilities, or with very long tunneling times. In the general case the total volume of the regions of space that has to be covered with the QTs grows in proportion to the size of the total space, which is exponential with respect to the number of dimensions, or particles. This helps to explain why QT formalism is unlikely to overcome the computational complexity of quantum mechanics.[68]

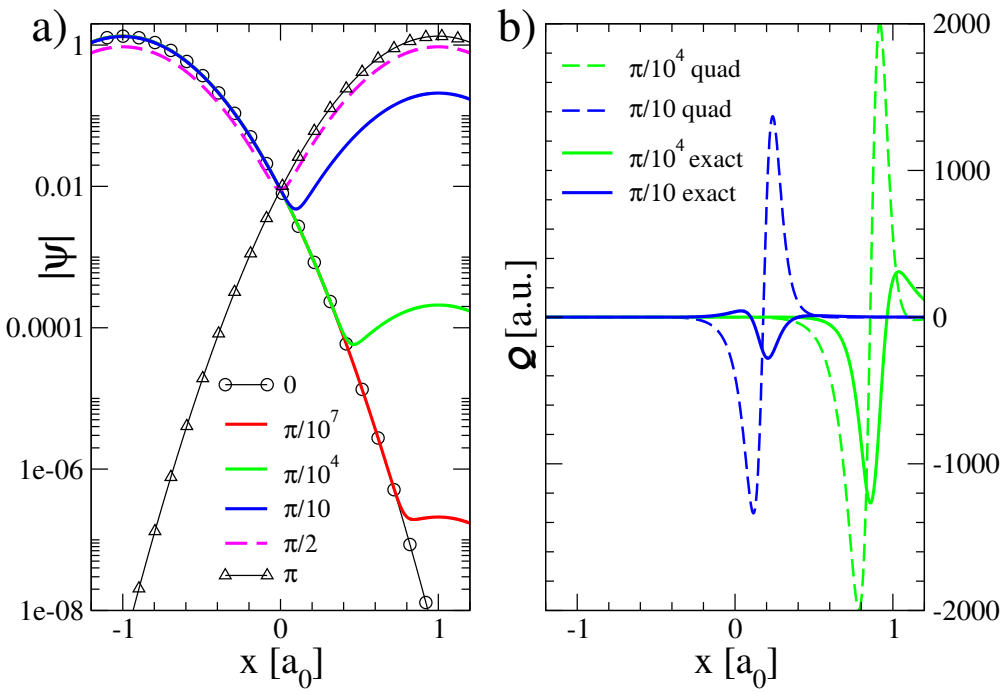


Figure 8: Dynamics in the model double well system for the initial wavepacket centered at $x = -1$ a$_0$. The wavefunction modulus, $|\psi|$ (on a logarithmic vertical scale) and $\mathcal{Q}$ (on a linear vertical scale) are shown in panels (a) and (b), respectively, as a function of coordinate $x$. $|\psi|$ is displayed for times $t = \{0, \pi/10^7, \pi/10^4, \pi/10\}$. Note, that the minimum develops far on the right at very short times in the region of low $|\psi|$, e.g. the $t = \pi/10^7$ curve, and drifts to the left during the dynamics. This feature is seen in the time-evolution of $\mathcal{Q}$, given at $t = \pi/10^4$ and $t = \pi/10$ as green and blue lines, respectively. The dashes of the same colors correspond to $\mathcal{Q}$ computed in the quadratic approximation.

## 3.4 Dynamics in the large mass limit

It is instructive to consider the energy flow in the semiclassical limit. In the development of approximate quantum trajectory methods targeting the semiclassical limit, we have previously argued for the "...limit of large mass for arbitrary physically reasonable initial wave function and kinetic energy density...".[69]

To implement this limit, we start with the reference particle mass $m_0$, and for simplicity set the GWP center parameters to zero, $\overline{x}_0 = 0,\ \overline{p}_0 = 0$. The initial width parameter of the GWP will be fixed to a real reference value, $A^{(0)}$, for all values of the particle mass $m \geq m_0$. The quadratic coefficient for the initial phase ($t = 0$) will depend on $m$ as follows,

$$A_0^{(m)} = A^{(0)} \left(1 + \imath\sqrt{m/m_0 - 1}\right). \tag{52}$$

This choice ensures that upon increase of mass, the total GWP energy is unchanged while the spacing between the energy levels is compressed. The classical limit is analyzed as the mass ratio $\lambda = m_0/m$ approaches zero. Using the time-dependence of the GWP parameters evolving in a parabolic potential $V = kx^2/2$ from Appendix 5, and introducing rescaled time $\tau$, width $\alpha$ and QT position $q$,

$$\tau = t\sqrt{k/m}, \quad \theta = \tan\tau, \quad \alpha = A^{(0)}/\sqrt{km_0}, \quad q_\tau = x\sqrt{A_{\Re}^{(m)}(t)}, \tag{53}$$

$\mathcal{Q}$ in this model is given by:

$$\mathcal{Q} = A_{\Re}A_{\Im}(1 - 2A_{\Re}x^2) = \frac{k(1-2q_\tau^2)}{m_0}\frac{\lambda^{3/2}\alpha\,(1+\theta^2)\left(\alpha(1-\theta^2)\sqrt{1-\lambda} + \theta\,(\alpha^2-1)\right)}{\left(\theta^2\alpha^2 + 2\,\theta\alpha\,\sqrt{1-\lambda} + 1\right)^2}. \tag{54}$$

The quantum measure $\mathcal{Q}$, evaluated at the parabola tip, $x = 0$, is shown in Fig. 9(a) as a function of the rescaled time $\tau$ for $\lambda = \{0.1, 0.01, 0.001\}$. The model parameters are taken as $m_0 = 1$ and $k = 1$ a.u. and the GWP reference width is equal to the coherent value $A^{(0)} = 1\ \mathrm{a}_0^{-2}$. As seen in the figure, as the particle mass increases ($\lambda \to 0$), the peaks become

narrower and their magnitude approaches a finite, non-zero limiting value, which shows that the quantum effects persist into the large mass limit.

The times $\tau_x$ of $\mathcal{Q}$ reaching its maximum/minimum values (at $q_\tau = 0$), to the leading order in $\lambda$, are determined from the following expression,

$$\tan\tau_x = \frac{1}{\alpha}\left(-\sqrt{1-\lambda} \pm \sqrt{\lambda/3}\right). \tag{55}$$

The extrema of $\mathcal{Q}$ as a function of $\tau$ obtained from Eq. (54) are, remarkably, independent of $\lambda$,

$$\mathcal{Q}_x = \mathcal{Q}|_{\tau=\tau_x} = \pm\frac{k}{m_0}\frac{3\sqrt{3}(1+\alpha^2)^2}{16\alpha^2}(1-2q^2_{\tau_x}). \tag{56}$$

Comparing the classical limit $\lambda \to 0$ of the time-dependent form of $\mathcal{Q}$ given by Eq. (54) with its extrema given by Eq. (56), we note that away from $\tau_x$, $\mathcal{Q}$ vanishes as $O(\lambda^{3/2})$. This is consistent with the premise of this work that the rate of change of the local energy operator describes local quantum effects in the system. At the extrema associated with the passage of the GWP through the near-focal points, the quantum effects do not vanish for any particle mass. The frequency of the focal point occurrence goes down with the particle mass increase as $m^{-1/2}$. At the limit of very large mass this happens increasingly rarely, but with the same magnitude. This suggests an interpretation of the semi-classical system as the one where quantum effects are 'rare' rather than 'small'.

We finish by examining the classical limit as described above for a popular mixed quantum/classical model,[45,70–72] consisting of the light particle of unit mass, harmonically bound to the heavy particle of mass $m$. The potential in atomic units is defined as:

$$V(x_1,x_2) = \frac{k_1}{2}(x_1-x_2)^2 + \frac{k_2}{2}x_2^2, \quad k_1 = 5, \quad k_2 = 15. \tag{57}$$

The reference mass for the heavy particle is set to $m_0 = 8.965$ a.u. The initial wavefunction is a factorizable two-dimensional Gaussian function given by Eq. (58) for the following

initial parameter values: $\overline{\boldsymbol{x}} = 0$, $\overline{\boldsymbol{p}} = 0$, $A_{11} = \sqrt{5}$, $A_{12} = 0$. The initial width parameter in the heavy particle dimension $x_2$ is $A_{22}^{(m_0)} = \sqrt{15 m_0}$ for the reference wavepacket, and it is $A_{22}^{(m)} = A_{22}^{(m_0)}(1 + \imath\sqrt{m/m_0 - 1})$, as in the one-dimensional case above. Presence of the quantum degree of freedom $x_1$ representing the light particle complicates the behavior of the system. To have well-defined extrema of the quantum power $\mathcal{Q}_x$, special values of $m$, producing periodic in time pattern of $\mathcal{Q}$ (due to resonant frequencies) were numerically found. The resulting $\mathcal{Q}_x$ are shown for these special values of $m$ in Fig. 9(b). The results are compared to those from uncoupled dynamics ($V = k_1 x_1^2/2 + k_2 x_2^2/2$) for the same initial wavepackets. As $m$ increases the minima and maxima become equal in magnitude, as true in the uncoupled case for all $m$. This trend shows that additional degrees of freedom do not 'wash out' the quantum features in the dynamics of the heavy particle. Therefore, our earlier conclusion, i.e. in the classical limit the quantum effects become rare rather than small, applies to the mixed quantum/classical systems.

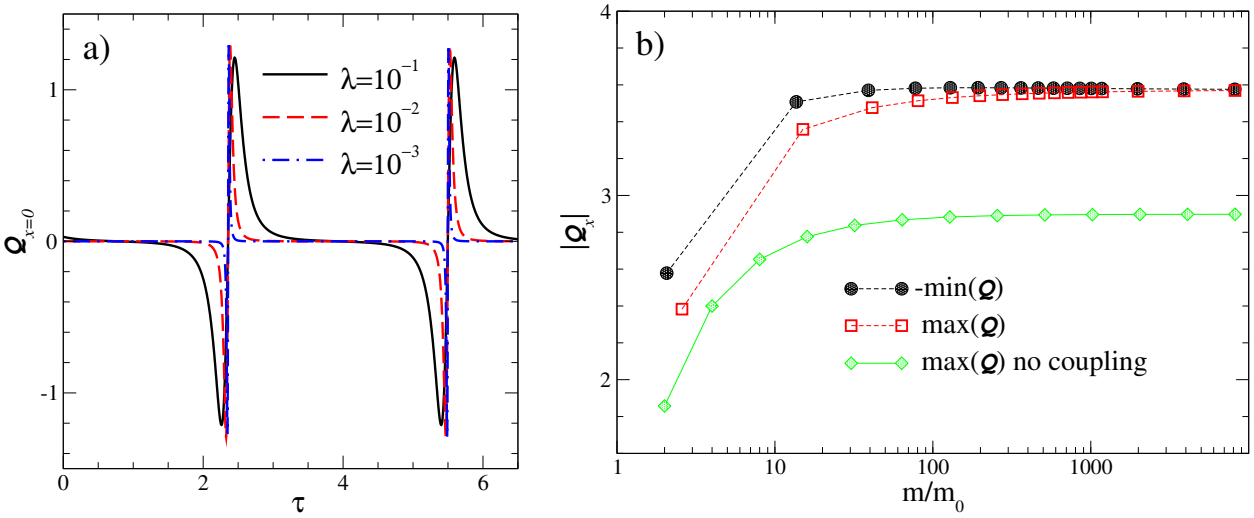


Figure 9: (a) The quantum power $\mathcal{Q}$, evaluated at $x = 0$, for a GWP in one dimension as a function of the rescaled time, $\tau$. The values of the mass ratio $\lambda = m_0/m$ are given in the legend. (b) The extrema of $\mathcal{Q}_x$ as a function of the relative mass of the heavy particle, $m/m_0$, for the two-dimensional quantum/classical model (Eq. (57)). The results from the uncoupled dynamics are displayed for comparison.

# 4 Conclusions

In this paper we have introduced a linear operator whose expectation value defines a quantum trajectory (QT). Essentially, it is a spherical (in Cartesian coordinates) Gaussian of vanishing width, whose center and width evolve according to the gradient and the hessian of the wavefunction phase. The symmetrized product of this operator with the Hamiltonian defines the local energy associated with the QT. The ratio of the expectation values of these operators defines the QT energy, whose time-derivative is the newly introduced *quantum power*, $\mathcal{Q}$, acting as a local measure of quantumness of a system evolving in time. We demonstrate that $\mathcal{Q}$ has no explicit dependence on the external potential, and vanishes in the classical limit $\hbar \to 0$, or when the local dynamics of the probability density flow is dominated by the forces from the external potential. The quantum power measure is "system-independent" or "universal", in the same sense as the universality of the exact exchange-correlation functional of the Density Functional Theory.[73]

We note that the concept of $\mathcal{Q}$ does not rely on *a priori* separation of total energy into the "quantum" and "classical" components. As such, it is not limited to the QT formalism and is applicable to other traditional quantum dynamics methods.

Computation of $\mathcal{Q}$ for the harmonic oscillator model demonstrates how the translational and the breathing motions of the Gaussian wavepacket (GWP) are facilitated by the loss of quantum energy at the trailing portions of the wavefunction, and gaining energy at the leading portions. Further application to the systems with prominent quantum interference, such as two GWPs, or two plane waves, demonstrates the complexity of $\mathcal{Q}$ and its singularity at the wavefunction nodes.

Analysis of $\mathcal{Q}$ in the tunneling models, i.e. the Eckart barrier and the deep double well, demonstrates the interpretive utility of $\mathcal{Q}$. When the GWP with the median energy below the barrier top, the interference between the incoming and the reflected portions of the GWP creates an interference pattern that transfers energy to some QTs, thus pushing them over the barrier. This process, while being challenging, can be described at the essentially

semiclassical level of QTs.[33,74,75] This is consistent with the current observation that the main features of $\mathcal{Q}$ at the early stages of tunnelling are observed on the side of the barrier with the incoming GWP. In contrast, analysis of the deep double well system shows that the main features of $\mathcal{Q}$ are formed at the initially empty side of the barrier. QTs are being 'pulled' through the barrier via the quantum energy redistribution among QTs at the leading tail of the wavefunction beyond the barrier. Such a process is hard to describe via QTs, as (consistent with very low probabilities or very long times for such processes) it requires coverage by QTs of the low-probability, essentially 'unpopulated' regions of the coordinate space. This is consistent with the known difficulties in describing the deep tunneling regime in the double well with QTs and time-dependent bases centered on classical trajectories.[7,76]

Furthermore, application of $\mathcal{Q}$ to the mixed quantum-classical 2D harmonic model, at the limit of large mass of the 'classical' particle demonstrates that the near singular features of $\mathcal{Q}$ do not vanish. The maximum value of $|\mathcal{Q}|$ approaches a constant. This maximum value is achieved at the times of resonance between the oscillations in the "quantum" and the "classical" degrees of freedom. This resonance happens increasingly rarely as mass of the "classical" particle increases. Our interpretation of this result is that the quantum features of dynamics become rare rather than small at the classical limit.

Finally, we reiterate that computation of $\mathcal{Q}$ near wavefunction nodes is numerically challenging due to the fourth order spatial derivatives. We took advantage of the analytic functional form combined with the high-accuracy solvers for the relevant equations of motion using Maple software, whenever possible, and we have used extra dense grids and small time-steps for the fully numerical wavefunction propagation. We speculate that some of the numerical difficulties will be alleviated in implementations where wavefunctions are represented within a basis of analytic functions, as commonly done in chemical applications.

# Appendix A: Evolution of a Gaussian wavepacket

A multidimensional Gaussian function of coordinates with time-dependent parameters solves the TDSE for a parabolic potential with possibly time-dependent coefficients. The solution known as a Gaussian wavepacket (GWP) or Thawed Gaussian[58] is given here for reference for an $N_d$-dimensional system described in Cartesian coordinates in atomic units ($\hbar = 1$),

$$\psi(\boldsymbol{x}, t) = N_0 \exp\left(-(\boldsymbol{x} - \overline{\boldsymbol{x}}_t)\mathbf{A}_t(\boldsymbol{x} - \overline{\boldsymbol{x}}_t)/2 + \imath\overline{\boldsymbol{p}}_t(\boldsymbol{x} - \overline{\boldsymbol{x}}_t) + \imath s_t + \gamma_t\right). \tag{58}$$

The subscript $t$ indicates functions dependent only on time $t$; it is omitted when unambiguous. $N_0$ is the initial normalization constant, so that initial value of the real scalar function $\gamma_t$ is set to zero, $\gamma_0 = 0$,

$$N_0 = \left(\frac{\det \Re(\mathbf{A}_0)}{\pi^{N_d}}\right)^{1/4}. \tag{59}$$

The wavefunction evolves according to the Hamiltonian,

$$\hat{H} = -\frac{1}{2}\hat{\boldsymbol{\nabla}}\mathbf{M}^{-1}\hat{\boldsymbol{\nabla}} + V(\boldsymbol{x}), \quad V(\boldsymbol{x}) = \frac{1}{2}\boldsymbol{x}\mathbf{V}_2\,\boldsymbol{x}, \tag{60}$$

$\mathbf{M}$ is a diagonal matrix of particle masses; $\mathbf{V}_2$ is a real symmetric matrix defining the quadratic potential $V(\boldsymbol{x})$, whose minimum is at the origin of the coordinate system and is equal to zero. In Eq. (58) the parameters $\overline{\boldsymbol{x}}_t$ and $\overline{\boldsymbol{p}}_t$ are real $N_d$-dimensional vectors, describing the GWP center. The real scalar function $s_t$ describes the coordinate-independent GWP phase. The remaining time-dependent functions form a *complex symmetric* matrix $\mathbf{A}_t$,

$$\mathbf{A}_t = \mathbf{A}_\Re + \imath\mathbf{A}_\Im,$$

with $\mathbf{A}_\Re$ defining the GWP width and $\mathbf{A}_\Im$ defining the quadratic phase of $\psi(\boldsymbol{x}, t)$.

Substituting Eq. (58) into the TDSE with the Hamiltonian (60), dividing the result by $\psi(\boldsymbol{x}, t)$ and setting imaginary and real coefficients, multiplying powers of $\boldsymbol{x}$, to zeroes, one

obtains the following equations determining the time-evolution of the parameters:

$$\begin{aligned}
\frac{d\overline{\boldsymbol{x}}}{dt} &= \mathbf{M}^{-1}\overline{\boldsymbol{p}}, \quad \frac{d\overline{\boldsymbol{p}}}{dt} = -\,\boldsymbol{\nabla} V|_{\boldsymbol{x}=\overline{\boldsymbol{x}}}\,, && (61)\\
\frac{ds}{dt} &= \frac{1}{2}\overline{\boldsymbol{p}}\;\mathbf{M}^{-1}\overline{\boldsymbol{p}} - V(\overline{\boldsymbol{x}}) - \mathcal{E}_0,\ \mathcal{E}_0 := \frac{1}{2}\,\mathrm{Tr}(\mathbf{A}_{\Re}\mathbf{M}^{-1}), && (62)\\
\frac{d\gamma}{dt} &= \frac{1}{2}\mathrm{Tr}(\mathbf{A}_{\Im}\mathbf{M}^{-1}), && (63)\\
\imath\frac{d\mathbf{A}}{dt} &= \mathbf{A}\mathbf{M}^{-1}\mathbf{A} - \mathbf{V}_2. && (64)
\end{aligned}$$

The last equation can be written for the real and imaginary parts separately as:

$$\begin{aligned}
\frac{d\boldsymbol{A}_{\Re}}{dt} &= (\mathbf{M}^{-1}\mathbf{A}_{\Im})^T\mathbf{A}_{\Re} + A_{\Re}\mathbf{M}^{-1}\mathbf{A}_{\Im}, && (65)\\
\frac{d\mathbf{A}_{\Im}}{dt} &= \mathbf{A}_{\Im}\mathbf{M}^{-1}\mathbf{A}_{\Im} - \mathbf{A}_{\Re}\mathbf{M}^{-1}\mathbf{A}_{\Re} + \mathbf{V}_2. && (66)
\end{aligned}$$

Eqs (61) are simply the Newton's equations of motion for the center of the Gaussian wavepacket, $\overline{\boldsymbol{x}}_t = \langle\psi|\boldsymbol{x}|\psi\rangle_t$. Thus, $\{\overline{\boldsymbol{x}}_t, \overline{\boldsymbol{p}}_t\}$ are the coordinates and momenta of a classical trajectory. Eq. (62) defines evolution of the classical action function $s_t$ along the center trajectory, except for the last rhs term, $\mathcal{E}_0$. For the ground state wavefunction, this term is equal to the ground state energy; thus, $\mathcal{E}_0$ is interpreted as the time-dependent generalization of the zero-point energy.

Finally, the time-dependence of $\mathbf{A}$ defines what is referred to as the breathing mode of the Gaussian, i.e. the change in localization of $|\psi(\boldsymbol{x},t)|$, with accompanying it quadratic phase. The change in $\mathbf{A}_{\Re}$ correlates with the time-dependence of $\gamma_t$, which ensures that the GWP norm remains constant in time, $\langle|\psi(\boldsymbol{x},t)|^2\rangle = 1$. For a special choice of $\mathbf{A}_0$, the GWP width remains constant in time, while the wavepacket center moves classically. Such a wavefunction is known as the coherent GWP: in the normal mode coordinates $\mathbf{A}$ is diagonal, $A_{nn} = m_n\omega_n$, where $\omega_n$ and $m_n$ are the frequency and mass of the $n^{th}$ normal mode.

The total GWP energy,

$$E = \langle \psi \hat{H} \psi \rangle = \frac{1}{2} \overline{\boldsymbol{p}}\ \mathbf{M}^{-1} \overline{\boldsymbol{p}} + V(\overline{\boldsymbol{x}}) + \frac{1}{2^{N_d}} \mathrm{Tr}(\mathbf{A}_{\Re}^{-1} \mathbf{V}_2) + \mathcal{K} + \mathcal{U}, \tag{67}$$

consists of the classical energy of the wavepacket center (first two rhs terms in Eq. (67)) and of the potential energy contribution due to the wavepacket delocalization (the third rhs term). The last two rhs terms, $\mathcal{K}$ and $\mathcal{U}$, denote the kinetic energy associated with the derivatives of the wavefunction phase and amplitude, respectively,

$$\mathcal{K} := \frac{1}{4} \mathrm{Tr}(\mathbf{A}_{\Im} \mathbf{A}_{\Re}^{-1} \mathbf{A}_{\Im} \mathbf{M}^{-1}), \quad \mathcal{U} := \frac{1}{4} \mathrm{Tr}(\mathbf{A}_{\Re} \mathbf{M}^{-1}). \tag{68}$$

$\mathcal{U}$ is equal to the expectation value of the quantum potential discussed in Section 2.1.

# Appendix B: Derivation of equation (37)

Let us derive the time dependence of the average local energy $\langle \hat{E}_W^\epsilon \rangle$ defined by Eqs (32) and (33),

$$\frac{\partial}{\partial t} \langle \hat{E}_W^\epsilon \rangle = \langle \frac{\partial \psi}{\partial t} \hat{E}_W^\epsilon \psi \rangle + \langle \psi \frac{\partial \hat{E}_W^\epsilon}{\partial t} \psi \rangle + \langle \psi \hat{E}_W^\epsilon \frac{\partial \psi}{\partial t} \rangle = \frac{-\imath}{\hbar} \langle \psi [\hat{E}_W^\epsilon, \hat{H}] \psi \rangle + \langle \psi \frac{\partial \hat{E}_W^\epsilon}{\partial t} \psi \rangle. \tag{69}$$

To simplify the analysis, we separate this expression into parts according to their dependence on the external potential $V$, since both the Hamiltonian and the local energy operators contain the terms proportional to $V$ and the terms independent of it. Denoting $\partial/\partial t = \partial_t$ and using the notations of Eqs (26-28), these terms are:

$$dE(V^2) := \frac{-\imath}{\hbar} \langle \psi [V g_W^\epsilon, V] \psi \rangle = 0 \tag{70}$$

$$dE(V) := \frac{\imath \hbar}{4} \langle \psi ([V g_W^\epsilon, 2\hat{\Delta}] + [g_W^\epsilon \hat{\Delta} + \hat{\Delta} g_W^\epsilon, V]) \psi \rangle + \langle \psi | V \partial_t g_W^\epsilon | \psi \rangle \tag{71}$$

$$dE(1) := \frac{-\imath \hbar^3}{8} \langle \psi [g_W^\epsilon \hat{\Delta} + \hat{\Delta} g_W^\epsilon, \hat{\Delta}] \psi \rangle + \frac{-\hbar^2}{4} \langle \psi (\partial_t g_W^\epsilon \hat{\Delta} + \hat{\Delta} \partial_t g_W^\epsilon) \psi \rangle. \tag{72}$$

The first term, given by Eq. (70), is equal to zero because it contains only the commutator of multiplicative functions. The next term (Eq. (71)) contains contributions from the commutator,

$$\begin{aligned} & \frac{\imath\hbar}{4}\langle\psi([V g_W^\epsilon, 2\hat{\Delta}] + [g_W^\epsilon\hat{\Delta} + \hat{\Delta} g_W^\epsilon, V])\psi\rangle \\ = \; & -\hbar^2 N_g \mathcal{A}_{\boldsymbol{q}_t}\Big(2V(\boldsymbol{\nabla}\mathcal{A}\cdot_m\boldsymbol{\nabla}S) + V\,\mathcal{A}\Delta S + \mathcal{A}(\boldsymbol{\nabla}V\cdot_m\boldsymbol{\nabla}S)\Big)_{\boldsymbol{q}_t} + O(\epsilon), \end{aligned} \tag{73}$$

and from the explicit time derivative,

$$\langle\psi|V\partial_t g_W^\epsilon|\psi\rangle = \hbar^2 N_g \mathcal{A}_{\boldsymbol{q}_t}\Big(2V(\boldsymbol{\nabla}\mathcal{A}\cdot_m\boldsymbol{\nabla}S) + \mathcal{A}(\boldsymbol{\nabla}V\cdot_m\boldsymbol{\nabla}S) + V\,\mathcal{A}\Delta S\Big)_{\boldsymbol{q}_t} + O(\epsilon). \tag{74}$$

The sum of Eqs (73) and (74) vanishes as $\epsilon \to 0$, $dE(V) = 0$. Therefore, the time-dependence of the local energy *expression* defined via $\hat{E}_W^\epsilon$ *is system-independent*, in other words, it does not depend on the forces acting on the quantum particles due to the classical external potential $V$.

The third term (Eq. (72)) contains contributions from the commutator,

$$\begin{aligned} - \; & \frac{\imath\hbar^3}{8}\langle\psi[g_W^\epsilon\hat{\Delta} + \hat{\Delta} g_W^\epsilon, \hat{\Delta}]\psi\rangle = \hbar^2 N_g \mathcal{A}_{\boldsymbol{q}_t}\Big(2\Delta(\boldsymbol{\nabla}S\cdot_m\boldsymbol{\nabla}\mathcal{A}) \\ + \; & (\boldsymbol{\nabla}\cdot_m\boldsymbol{\nabla}S)\Delta\mathcal{A} - 2\,\mathrm{Tr}(\mathbf{M}^{-1}[\boldsymbol{\nabla}\otimes\boldsymbol{\nabla}\mathcal{A}]\mathbf{M}^{-1}[\boldsymbol{\nabla}\otimes\boldsymbol{\nabla}S]) + \frac{\mathcal{A}}{2}\Delta(\boldsymbol{\nabla}\cdot_m\boldsymbol{\nabla}S) \\ - \; & \frac{1}{\hbar^2}\Big(\mathcal{A}\Delta S(\boldsymbol{\nabla}S\cdot_m\boldsymbol{\nabla}S) + \mathcal{A}(\boldsymbol{\nabla}S\cdot_m\boldsymbol{\nabla})(\boldsymbol{\nabla}S\cdot_m\boldsymbol{\nabla}S) + 2(\boldsymbol{\nabla}\mathcal{A}\cdot_m\boldsymbol{\nabla}S)(\boldsymbol{\nabla}S\cdot_m\boldsymbol{\nabla}S)\Big)\Big)_{\boldsymbol{q}_t}, \end{aligned} \tag{75}$$

and from the explicit time derivative,

$$\begin{aligned} & -\frac{\hbar^2}{4}\langle\psi(\partial_t g_W^\epsilon\hat{\Delta} + \hat{\Delta}\partial_t g_W^\epsilon)\psi\rangle = \hbar^2 N_g\Big(-\Delta\mathcal{A}(\boldsymbol{\nabla}S\cdot_m\boldsymbol{\nabla}\mathcal{A}) - \mathcal{A}\Delta S\Delta\mathcal{A} - \mathcal{A}(\boldsymbol{\nabla}S\cdot_m\boldsymbol{\nabla})\Delta\mathcal{A} \\ & + \frac{1}{\hbar^2}\Big(2\mathcal{A}(\boldsymbol{\nabla}\mathcal{A}\cdot_m\boldsymbol{\nabla}S)(\boldsymbol{\nabla}S\cdot_m\boldsymbol{\nabla}S) + \mathcal{A}^2(\boldsymbol{\nabla}S\cdot\boldsymbol{\nabla}(\boldsymbol{\nabla}S\cdot\boldsymbol{\nabla}S)) + \mathcal{A}^2\,\Delta S(\boldsymbol{\nabla}S\cdot_m\boldsymbol{\nabla}S)\Big)\Big)_{\boldsymbol{q}_t} + O(\epsilon). \end{aligned} \tag{76}$$

Eqs (75) and (76) add up to:

$$\begin{aligned}\frac{\partial}{\partial t}\langle\hat{E}^{\epsilon}_{W}\rangle &= \hbar^2 N_g\Big(2\mathcal{A}(\Delta(\boldsymbol{\nabla}S\cdot_m\boldsymbol{\nabla}\mathcal{A}))-\Delta\mathcal{A}(\boldsymbol{\nabla}S\cdot_m\boldsymbol{\nabla}\mathcal{A}) \\ &- 2\mathcal{A}\ \mathrm{Tr}(\mathbf{M}^{-1}[\boldsymbol{\nabla}\otimes\boldsymbol{\nabla}\mathcal{A}]\mathbf{M}^{-1}[\boldsymbol{\nabla}\otimes\boldsymbol{\nabla}S])+\frac{\mathcal{A}^2}{2}\Delta\Delta S-\mathcal{A}(\boldsymbol{\nabla}S\cdot_m\boldsymbol{\nabla})\Delta\mathcal{A}\Big)_{\boldsymbol{q}_t}.\end{aligned} \tag{77}$$

# 5 Supporting Information

Description of the supplementary files [SI-cover.docx]

Verification of the analytic derivation of Eq. (39) [SI-1.txt]

Analytic solution for the interference of two Gaussian wavepackets of Section 3.2.1 [SI-2.txt]

Analytic solution for the deep tunneling model of Section 3.3.2 [SI-3.txt]

# 6 Acknowledgments

This work was supported in part by the National Science Foundation under Grant CHE-1955768 and by the NSF EPSCoR Program under Award OIA-1655740/20-GC03. Any opinions, findings and conclusions or recommendations expressed in this material are those of the authors and do not necessarily reflect those of the National Science Foundation.

# References

(1) Worth, G. A. Quantics: A general purpose package for Quantum molecular dynamics simulations. *Comput. Phys. Commun.* **2020**, *248*, 107040.

(2) Pandey, A.; Poirier, B. Using phase-space Gaussians to compute the vibrational states of OCHCO+. *J. Chem. Phys.* **2019**, *151*, 014114.

(3) Markland, T. E.; Ceriotti, M. Nuclear quantum effects enter the mainstream. *Nat. Rev. Chem.* **2018**, *2*, 0109.

(4) Gatti, F., Ed. *Molecular Quantum Dynamics: from theory to applications*; Springer, 2014.

(5) Flynn, S. W.; Mandelshtam, V. A. Sampling general distributions with quasi-regular grids: Application to the vibrational spectra calculations. *J. Chem. Phys.* **2019**, *151*, 241105.

(6) Dutra, M.; Wickramasinghe, S.; Garashchuk, S. Quantum Dynamics with the Quantum Trajectory-Guided Adaptable Gaussian Bases. *J. Chem. Theory Comput.* **2020**, *16*, 18–34.

(7) Saller, M. A. C.; Habershon, S. Quantum Dynamics with Short-Time Trajectories and Minimal Adaptive Basis Sets. *J. Chem. Theory Comput.* **2017**, *13*, 3085–3096.

(8) Wang, L.; Akimov, A.; Prezhdo, O. V. Recent Progress in Surface Hopping: 2011-2015. *J. Phys. Chem. Lett.* **2016**, *7*, 2100–2112.

(9) Karplus, M.; Porter, R. N.; Sharma, R. D. Exchange Reactions with Activation Energy. I. Simple Barrier Potential for (H, H2). *J. Chem. Phys.* **1965**, *43*, 3259–3287.

(10) Schatz, G. C. Perspective on "Exchange reactions with activation energy. I. Simple barrier potential for (H, H-2)" - Karplus M, Porter RN, Sharma RD (1965) J Chem Phys 43 : 3259-3287. *Theor. Chem. Acc.* **2000**, *103*, 270–272.

(11) Schatz, G. C.; Bowman, J. M.; Kuppermann, A. Exact quantum, quasiclassical, and semiclassical reaction probabilities for collinear $F+D_2 \rightarrow FD+D$ reaction. *J. Chem. Phys.* **1975**, *63*, 685–696.

(12) Schatz, G. C. The origin of cross section thresholds in H+H2: Why quantum dynamics appears to be more vibrationally adiabatic than classical dynamics. *J. Chem. Phys* **1983**, *79*, 5386–5391.

(13) Czako, G.; Kaledin, A. L.; Bowman, J. M. A practical method to avoid zero-point leak in molecular dynamics calculations: Application to the water dimer. *J. Chem. Phys.* **2010**, *132*.

(14) Shu, Y.; Dong, S. S.; Parker, K. A.; Bao, J. L.; Zhang, L.; Truhlar, D. G. Extended Hamiltonian molecular dynamics: semiclassical trajectories with improved maintenance of zero point energy. *Phys. Chem. Chem. Phys.* **2018**, *20*, 30209–30218.

(15) Nandi, A.; Zhang, P.; Chen, J.; Guo, H.; Bowman, J. M. Quasiclassical simulations based on cluster models reveal vibration-facilitated roaming in the isomerization of CO adsorbed on NaCl. *Nat. Chem.* **2021**, *13*, 249–254.

(16) Webster, F.; Light, J. C. Atom-Diatom Reactive Scattering. I. Quantum Theory. *J. Chem. Phys.* **1989**, *90*, 265.

(17) Tannor, D. J.; Weeks, D. E. Wave packet correlation-function formulation of scattering theory – The quantum analog of classical S-matrix theory. *J. Chem. Phys.* **1993**, *98*, 3884–3893.

(18) Miller, W. H. Semiclassical Theory of Atom–Diatom Collisions: Path Integrals and the Classical S Matrix. *J. Chem. Phys.* **1970**, *53*, 1949–1959.

(19) Miller, W. H. Quantum-mechanical transition-state theory and a new semiclassical model for reaction-rate constants. *J. Chem. Phys.* **1974**, *61*, 1823–1834.

(20) Heller, E. J. Time-dependent approach to semiclassical dynamics. *J. Chem. Phys.* **1975**, *62*, 1544–1555.

(21) Herman, M. F.; Kluk, E. A semiclassical justification for the use of non-spreading wavepackets in dynamics calculations. *Chem. Phys.* **1984**, *91*, 27.

(22) Kay, K. G. Integral expressions for the semiclassical time-dependent propagator. *J. Chem. Phys.* **1994**, *100*, 4377–4392.

(23) Werther, M.; Choudhury, S. L.; Grossmann, F. Coherent state based solutions of the time-dependent Schrödinger equation: hierarchy of approximations to the variational principle. *Int. Rev. Phys. Chem.* **2021**, *40*, 81–125.

(24) Tully, J. C. Mixed quantum-classical dynamics. *Faraday Discuss.* **1998**, *110*, 407–419.

(25) Ben-Nun, M.; Quenneville, J.; Martinez, T. J. Ab initio multiple spawning: Photochemistry from first principles quantum molecular dynamics. *J. Chem. Phys.* **2001**, *104*, 5161–5175.

(26) Romer, S.; Burghardt, I. Towards a variational formulation of mixed quantum-classical molecular dynamics. *Mol. Phys.* **2013**, *111*, 3618.

(27) Otto, F. Multi-layer Potfit: An accurate potential representation for efficient high-dimensional quantum dynamics. *J. Chem. Phys.* **2014**, *140*.

(28) Dawes, R.; Passalacqua, A.; Wagner, A. F.; Sewell, T. D.; Minkoff, M.; Thompson, D. L. Interpolating moving least-squares methods for fitting potential energy surfaces: Using classical trajectories to explore configuration space. *J. Chem. Phys.* **2009**, *130*, 144107.

(29) Richings, G. W.; Habershon, S. Direct Quantum Dynamics Using Grid-Based Wave Function Propagation and Machine-Learned Potential Energy Surfaces. *J. Chem. Theory Comput.* **0**, *0*, null.

(30) Vreven, T.; Byun, K. S.; Komaromi, I.; Dapprich, S.; Montgomery, J. A.; Morokuma, K.; Frisch, M. J. Combining quantum mechanics methods with molecular mechanics methods in ONIOM. *J. Chem. Theory Comput.* **2006**, *2*, 815–826.

(31) Bohm, D. A suggested interpretation of the quantum theory in terms of "hidden" variables, I and II. *Phys. Rev.* **1952**, *85*, 166–193.

(32) Wyatt, R. E. *Quantum Dynamics with Trajectories: Introduction to Quantum Hydrodynamics*; Springer-Verlag, 2005.

(33) Garashchuk, S.; Rassolov, V. A. Energy conserving approximations to the quantum potential: Dynamics with linearized quantum force. *J. Chem. Phys.* **2004**, *120*, 1181–1190.

(34) Garashchuk, S.; Jakowski, J.; Rassolov, V. A. Approximate quantum trajectory dynamics for reactive processes in condensed phase. *Molecular Simulation* **2015**, *41*, 1–21.

(35) Garashchuk, S.; Rassolov, V. Quantum Trajectory Dynamics Based on Local Approximations to the Quantum Potential and Force. *J. Chem. Theory Comput.* **2019**, *15*, 3906–3916.

(36) Garashchuk, S.; Rassolov, V. A. Quantum dynamics with Bohmian trajectories: Energy conserving approximation to the quantum potential. *Chem. Phys. Lett.* **2003**, *376*, 358–363.

(37) Rassolov, V. A.; Garashchuk, S.; Schatz, G. C. Quantum trajectory dynamics in arbitrary coordinates. *J. Phys. Chem. A* **2006**, *110*, 5530–5536.

(38) Zhao, Y.; Makri, N. Bohmian versus semiclassical description of interference phenomena. *J. Chem. Phys.* **2003**, *119*, 60–67.

(39) Babyuk, D.; Wyatt, R. E. Coping with the node problem in quantum hydrodynamics: the covering function method. *J. Chem. Phys.* **2004**, *121*, 9230–9238.

(40) Kendrick, B. K. An iterative finite difference method for solving the quantum hydrodynamic equations of motion. *J. Mol. Structure-Theochem* **2010**, *943*, 158–167.

(41) Garashchuk, S.; Rassolov, V. A. Modified quantum trajectory dynamics using a mixed wavefunction representation. *J. Chem. Phys.* **2004**, *121*, 8711–8715.

(42) Kempe, J.; Kitaev, A.; Regev, O. The complexity of the local hamiltonian problem. *SIAM J. Comput.* **2006**, *35*, 1070–1097.

(43) Garashchuk, S.; Rassolov, V. A. Stable long-time semiclassical description of zero-point energy in high-dimensional molecular systems. *J. Chem. Phys.* **2008**, *129*, 024109.

(44) Burant, J. C.; Tully, J. C. Nonadiabatic dynamics via the classical limit Schrödinger equation. *J. Chem. Phys.* **2000**, *112*, 6097–6103.

(45) Garashchuk, S.; Volkov, M. V. The energy-conserving dynamics of quantum-classical systems based on quantum trajectories. *Mol. Phys.* **2012**, *110*, 985–993.

(46) Curchod, B. F. E.; Tavernelli, I.; Rothlisberger, U. Trajectory-based solution of the nonadiabatic quantum dynamics equations: an on-the-fly approach for molecular dynamics simulations. *Phys. Chem. Chem. Phys.* **2011**, *13*, 3231–3236.

(47) Gu, B.; Franco, I. Partial hydrodynamic representation of quantum molecular dynamics. *J. Chem. Phys.* **2017**, *146*.

(48) Talotta, F.; Agostini, F.; Ciccotti, G. Quantum Trajectories for the Dynamics in the Exact Factorization Framework: A Proof-of-Principle Test. *J. Phys. Chem. A* **2020**, *124*, 6764–6777.

(49) Burghardt, I.; Parlant, G. On the dynamics of coupled Bohmian and phase-space variables: A new hybrid quantum-classical approach. *J. Chem. Phys.* **2004**, *120*, 3055–3058.

(50) Smith, B.; Akimov, A. V. Entangled trajectories Hamiltonian dynamics for treating quantum nuclear effects. *J. Chem. Phys.* **2018**, *148*.

(51) Sanz, A. S.; Borondo, F.; Miret-Artes, S. Particle diffraction studied using quantum trajectories. *J. Phys.* **2002**, *14*, 6109–6145.

(52) Sanz, A. S.; Miret-Artés, S. A causal look into the quantum Talbot effect. *J. Chem. Phys.* **2007**, *126*, 234106.

(53) Holland, P. R. *The quantum theory of motion*; Cambridge University Press, 1993.

(54) Sanz, A. S.; Miret-Artes, S. *A Trajectory Description of Quantum Processes. I. Fundamentals: A Bohmian Perspective*; Lecture Notes in Physics; Springer, 2012; Vol. 850.

(55) Sanz, A. S.; Miret-Artes, S. *A Trajectory Description of Quantum Processes. II. Applications: A Bohmian Perspective*; Lecture Notes in Physics; Springer, 2014; Vol. 831.

(56) Heller, E. J. Wigner phase space method: Analysis for semiclassical applications. *J. Chem. Phys.* **1976**, *65*, 1289–1298.

(57) Heller, E. J. Classical limit of the Liouville equation. *J. Chem. Phys.* **1976**, *65*, 1289.

(58) Tannor, D. J. *Introduction to Quantum Mechanics: A Time-Dependent Perspective*; University Science Books, 2006.

(59) Feit, M. D.; Fleck, J. A.; Steiger, A. *J. Comp. Phys.* **1982**, *47*, 412.

(60) Kosloff, R. Time-dependent quantum-mechanical methods for molecular dynamics. *J. Phys. Chem.* **1988**, *92*, 2087–2100.

(61) Tonomura, A.; Endo, J.; Matsuda, T.; Kawasaki, T.; Ezawa, H. Demonstration of single-electron buildup of an interference pattern. *Am. J. Phys.* **1989**, *57*, 117–120.

(62) Sanz, A. S.; Miret-Artés, S. A trajectory-based understanding of quantum interference. *J. Phys. A.* **2008**, *41*, 435303.

(63) Chou, C.-C.; Sanz, A. S.; Miret-Artés, S.; Wyatt, R. E. Hydrodynamic View of Wave-Packet Interference: Quantum Caves. *Phys. Rev. Lett.* **2009**, *102*, 250401.

(64) Garashchuk, S.; Rassolov, V. A. Semiclassical dynamics based on quantum trajectories. *Chem. Phys. Lett.* **2002**, *364*, 562–567.

(65) Donoso, A.; Yeng, Y. J.; Martens, C. C. Simulation of quantum processes using entangled trajectory molecular dynamics. *J. Chem. Phys.* **2003**, *119*, 5010–5020.

(66) Maddox, J. B.; Bittner, E. R. Estimating Bohm's quantum force using Bayesian statistics. *J. Chem. Phys.* **2003**, *119*, 6465–6474.

(67) Min, S. K.; Agostini, F.; Tavernelli, I.; Gross, E. K. U. Ab Initio Nonadiabatic Dynamics with Coupled Trajectories: A Rigorous Approach to Quantum (De)Coherence. *J. Phys. Chem. Lett.* **2017**, *8*, 3048–3055.

(68) V. A. Rassolov and S. Garashchuk, Computational complexity in quantum chemistry. *Chem. Phys. Lett.* **2008**, *464*, 262–264.

(69) Rassolov, V. A.; Garashchuk, S. Semiclassical nonadiabatic dynamics with quantum trajectories. *Phys. Rev. A* **2005**, *71*, 032511.

(70) Kohen, D.; Stillinger, F. H.; Tully, J. C. Model studies of nonadiabatic dynamics. *J. Chem. Phys.* **1998**, *109*, 4713–4725.

(71) Prezhdo, O. V.; Brooksby, C. Quantum backreaction through the Bohmian particle. *Phys. Rev. Lett.* **2001**, *86*, 3215–3219.

(72) Gindensperger, E.; Meier, C.; Beswick, J. A.; Heitz, M. C. Quantum-classical description of rotational diffractive scattering using Bohmian trajectories: Comparison with full quantum wave packet results. *J. Chem. Phys.* **2002**, *116*, 10051–10059.

(73) Kohn, W. Nobel Lecture: Electronic structure of matter—wave functions and density functionals. *Rev. Mod. Phys.* **1999**, *71*, 1253–1266.

(74) Lopreore, C. L.; Wyatt, R. E. Quantum wave packet dynamics with trajectories. *Phys. Rev. Lett.* **1999**, *82*, 5190–5193.

(75) Donoso, A.; Martens, C. C. Quantum tunneling using entangled classical trajectories. *Phys. Rev. Lett.* **2001**, *87*, 223202(1–4).

(76) Ronto, M.; Shalashilin, D. V. Numerical Implementation and Test of the Modified Variational Multiconfigurational Gaussian Method for High-Dimensional Quantum Dynamics. *J. Phys. Chem. A* **2013**, *117*, 6948–6959.

# Graphical TOC Entry